DYNAMICS AND CONTROL OF DUAL-HOIST CRANES MOVING DISTRIBUTED PAYLOADS

A Thesis
Presented to
The Academic Faculty

by

Alexander S. Miller

In Partial Fulfillment
of the Requirements for the Degree
Master of Science in Mechanical Engineering in the
The George W. Woodruff School of Mechanical Engineering

Georgia Institute of Technology
December 2015

Copyright © 2015 by Alexander S. Miller

DYNAMICS AND CONTROL OF DUAL-HOIST CRANES MOVING DISTRIBUTED PAYLOADS

Approved by:

Professor William Singhose, Advisor
The George W. Woodruff School of
Mechanical Engineering
Georgia Institute of Technology

Professor Jun Ueda
The George W. Woodruff School of
Mechanical Engineering
Georgia Institute of Technology

Professor Nader Sadegh
The George W. Woodruff School of
Mechanical Engineering
Georgia Institute of Technology

Date Approved: November 24, 2015

ACKNOWLEDGEMENTS

I would like to thank God for all he has given me. I would like to thank my parents, Stephen and Nancy, for their love and support. I would like to thank my girlfriend, Morgan, for her loving encouragement and patience during my graduate studies.

I would like to thank my advisor, Dr. William Singhose, for his encouragement, support, and guidance. I would also like to thank my committee members, Dr. Ueda and Dr. Sadegh, for their support of this work. I would like to thank Caroline Rhee for her work with the human operator testing.

TABLE OF CONTENTS

LIST OF TABLES

LIST OF FIGURES

SUMMARY

Crane motion induces payload oscillation that makes accurate positioning of the payload a challenging task. As the payload size increases, it may be necessary to utilize multiple cranes for better control of the payload position and orientation. However, simultaneously maneuvering multiple cranes to transport a single payload increases the complexity and danger of the operation.

This thesis investigates the dynamics and control of dual-hoist bridge cranes transporting distributed payloads. Insights from this dynamic analysis were used to design input shapers that reduce payload oscillation originating from various crane motions. Also, studies were conducted to investigate the effect input shaping has on the performance of human operators using a dual-hoist bridge crane to transport distributed payloads through an obstacle course. In each study, input shaping significantly improved the task completion time. Furthermore, input-shaping control greatly decreased operator effort, as measured by the number of interface button pushes needed to complete a task. These results clearly demonstrate the benefit of input-shaping control on dual-hoist bridge cranes.

In addition, a new system identification method that utilizes input shaping for determining the modal frequencies and relative amplitude contributions of individual modes was developed to aid in the dynamic analysis of dual-hoist bridge cranes, as well as other multi-mode systems. This method uses a new type of input shaper to suppress all but one mode to a low level. The shaper can also be used to bring a small-amplitude mode to light by modifying one of the vibration constraints.

CHAPTER I

INTRODUCTION

1.1 Motivation

Cranes are used to transport heavy loads in manufacturing facilities, at shipyards, throughout nuclear sites, and during construction of buildings. All of these industries value throughput and safety. However, crane motion induces payload oscillation that makes accurate positioning of the payload a challenging task. Excessive payload sway can result in collisions that damage equipment or injure people. A large payload that swings outward from the base of a crane can also greatly increase the tipping moment and lead to catastrophic collapse of the crane. To increase safety, cranes are often driven slowly, at the expense of throughput, and the payloads are manually constrained with ropes to avoid large swings.

Controlling distributed-mass payloads with a single-hoist crane can be challenging because the payload can oscillate like a double-pendulum and twist about the rigging cables [7]. As the payload size increases, it may be necessary to utilize multiple cranes to better control the payload orientation. For example, Figure 1.1 shows two mobile cranes hoisting a blade assembly during the erection of a wind turbine[1]. If a payload exceeds the weight capacity of a single crane, then two cranes could also be used to perform a tandem lift. However, simultaneously maneuvering multiple cranes to lift a single payload increases the complexity and danger of the operation [3, 28].

Along with objects at the worksite, each crane must also avoid collisions with the other moving cranes. The orientation of the payload is affected by the movement

[1]Stewart, Ashley. 2010. Web. 20 May 2015. Appears in: Stewart, Ashley. (2010, August 26). Topping a Tower. *Albert Lea Tribune*

Figure 1.1: Erection of Wind Turbine[1]

of each crane. Poorly executed moves can result in a configuration that causes one or more cranes to collapse or tip over [27, 26, 11, 25]. Understanding the complex response of multi-hoist cranes as a function of various inputs and configurations is an important step in controlling them effectively.

1.2 Dual-Hoist Bridge Crane

Dual-hoist bridge cranes are the subject of this thesis. This type of crane has two controllable attachment points that provide additional control of the payload orientation, compared to single-hoist cranes. This section describes the physical crane used for experiments and a numerical model used for performing simulations.

1.2.1 Physical Crane

Figure 1.2a shows the dual-hoist bridge crane carrying a triangular payload. The crane operates in a 10 m x 8.5 m x 2.6 m workspace. The two overhead trolleys can move independently (or dependently) along a bridge. Each trolley is capable of lifting up to 1 ton. The bridge itself can travel along rails (not shown) attached along either

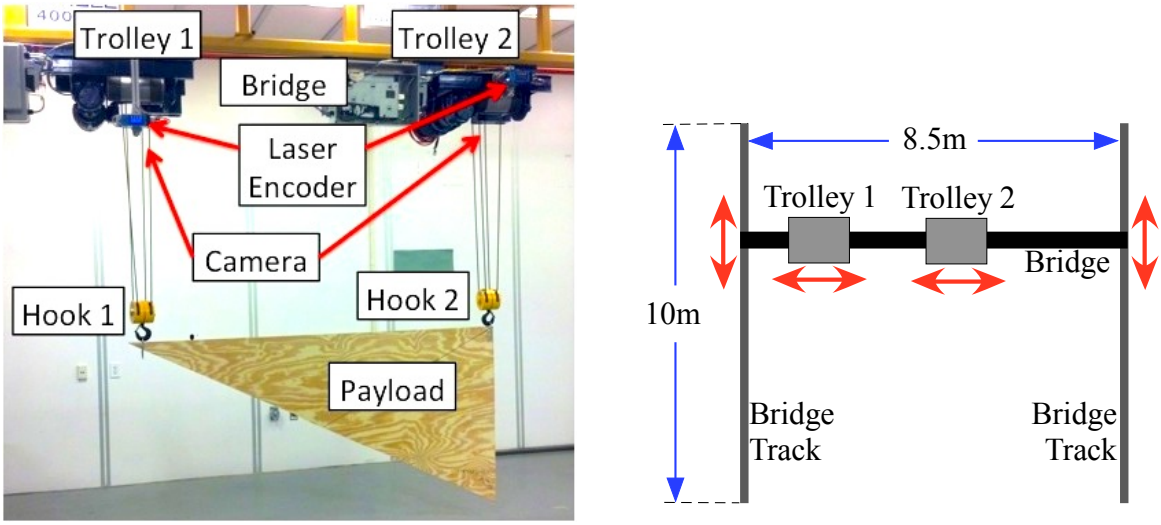

(a) Annotated Photograph **(b)** Overhead Schematic

Figure 1.2: Dual-Hoist Bridge Crane

side of the ceiling. The configuration is illustrated by the overhead schematic shown in Figure 1.2b.

All motions of the trolleys and bridge are controlled by Siemens SIMOTION drives. Supervisory control of the system is provided by a Programmable Logic Controller (PLC). The PLC and drives communicate wirelessly through Siemens wireless access points. The positions of the trolleys and bridge in the workspace are determined by laser encoders attached to the trolleys and one end of the bridge, respectively. The hook motions are measured using downward-pointing Cognex cameras attached to the bottom of the trolleys. Table 1.1 summarizes the important parameters of the crane shown in Figure 1.2a.

1.2.2 Numerical Model

A two-dimensional sketch of the dual-hoist bridge crane is shown in Figure 1.3. The trolleys can move in the y direction, along a line that passes through the trolleys. Each trolley has a hook attached at the end of its suspension cable. The hook masses of trolley 1 and trolley 2 are M_{H1} and M_{H2}, respectively. The suspension cables are treated as massless, rigid bodies. The length of the trolley 1 suspension cable is

Table 1.1: Dual-Hoist Crane Parameters

Parameter	**Value**
Workspace	10 m x 8.5 m x 2.6 m
Total Load Capacity	2 tons
Hook Mass, M_{H1} and M_{H2}	7.65 kg
Max. Cable Length	2.6 m
Min. Trolley Separation	1.65 m
Max. Trolley Acceleration & Velocity	1 m/s^2; 0.33 m/s
Max. Bridge Acceleration & Velocity	1 m/s^2; 0.33 m/s

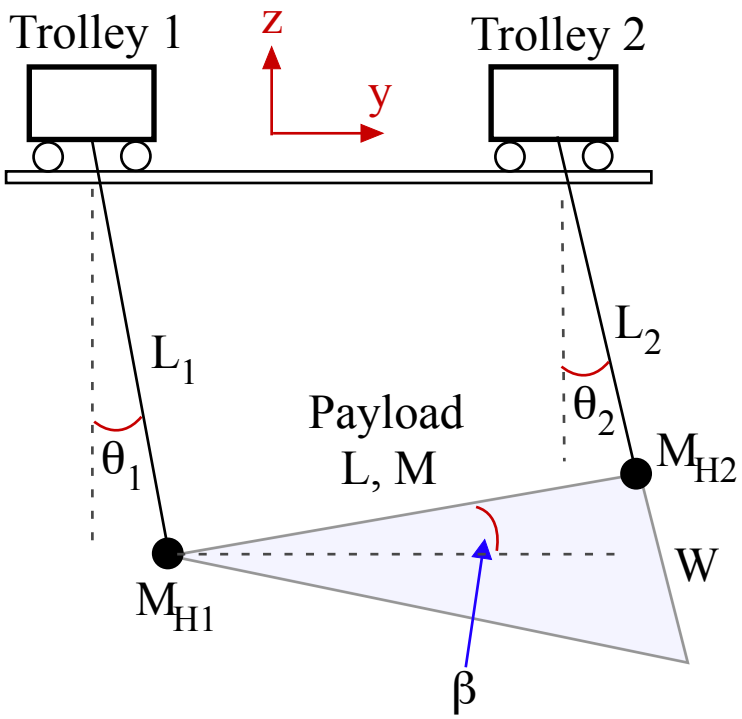

Figure 1.3: 2-D Dual-Hoist Bridge Crane Model

L_1, and it can swing relative to its suspension point from trolley 1 by an angle θ_1. The length of the trolley 2 suspension cable is L_2, and it can rotate by an angle θ_2. The triangular payload has a length L, width W, and mass M. The payload can be rotated about an axis perpendicular to the bridge axis and the vertical direction. This rotation can be considered a pitch angle β.

A three-dimensional sketch of a dual-hoist bridge crane is shown in Figure 1.4. The trolleys can also move in the x direction, perpendicular to the y direction. Motion

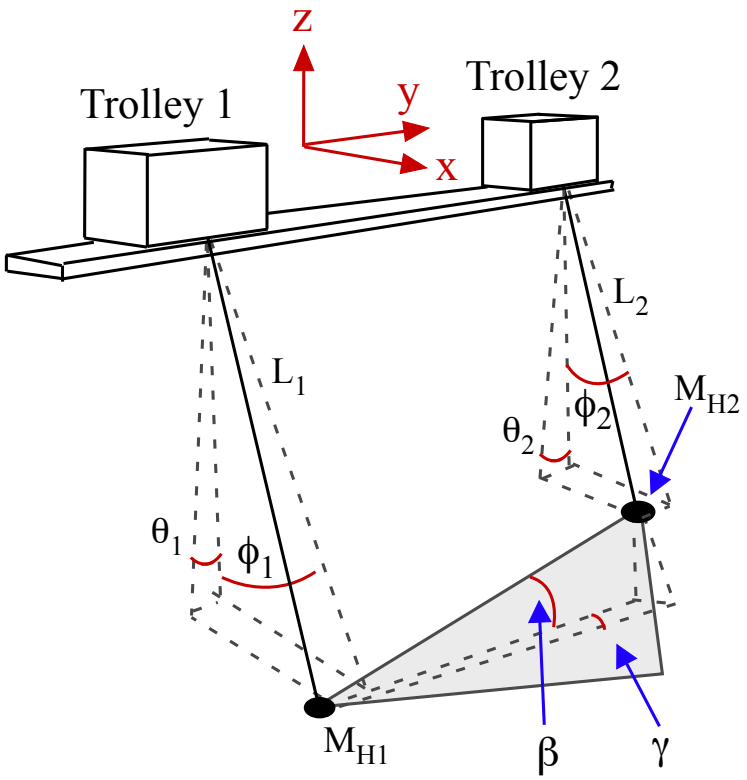

Figure 1.4: 3-D Dual-Hoist Bridge Crane Model

in this perpendicular direction is called bridge motion. The trolley 1 suspension cable can swing relative to its suspension point from trolley 1 about an axis parallel to the y direction by an angle ϕ_1. The trolley 2 suspension cable can rotate by an angle ϕ_2.

Figure 1.5 shows the payload rotation angles. The pitch angle, β, is shown in Figure 1.5a. From a top view perspective, the twist angle γ is created by the intersection of the line connecting the two trolleys with the line connecting the two hooks. In Figure 1.5b, the payload is rotated to demonstrate γ from a side view perspective, with dashed lines representing a projection of the line connecting the two trolleys (trolleys not shown) and the line connecting the two hooks. Finally, the payload is free to rotate about an axis that connects the two hooks through the roll angle ψ, as shown in Figure 1.5c.

The inputs to the model are the accelerations of the two trolleys in the trolley-motion direction, $\ddot{y}_1$ and $\ddot{y}_2$, and bridge-motion direction, $\ddot{x}_1$ and $\ddot{x}_2$. The model

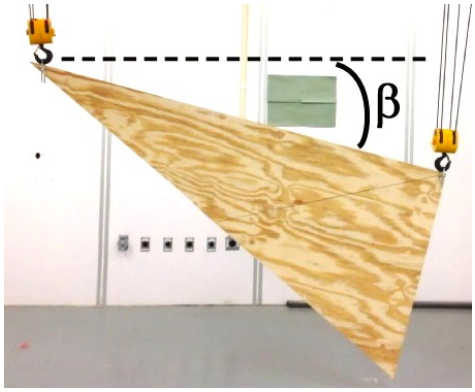

(a) Pitch Angle, β

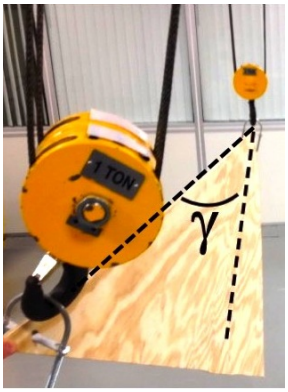

(b) Twist Angle, γ

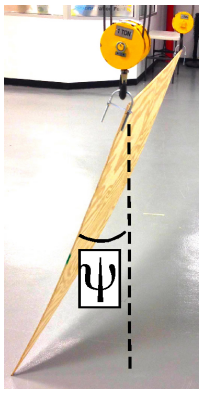

(c) Roll Angle, ψ

Figure 1.5: Payload Rotation Angles

Table 1.2: Nominal Dual-Hoist Crane Simulation Parameters

Parameter	**Value**
Payload Mass, M	7 kg
Payload Length, L	2.3 m
Payload Width, W	1.2 m
Hook Cable Lengths, L_1 and L_2	1.5 m
Hook Masses, M_{H1} and M_{H2}	7.65 kg
Trolley Separation Distance	2.3 m
Max. Trolley Acceleration & Velocity	1 m/s^2; 0.33 m/s
Max. Bridge Acceleration & Velocity	1 m/s^2; 0.33 m/s

is similar to a hanging four-bar mechanism with two moveable support points (the two trolleys). But, the payload "bar" can twist, as measured by the twist angle γ. The mathematical model for this system was obtained using the commercial dynamics package, MotionGenesis [1]. The computer code is listed in Appendix A. The nominal simulation parameters are shown in Table 1.2.

The baseline reference motion command used in this investigation is a trapezoidal-velocity profile (bang-coast-bang acceleration) because it utilizes the maximum acceleration and velocity specified in the control program. Furthermore, trapezoidal velocity profiles mimic the commands issued by crane operators through standard

push-button pendents. For small motions, the trapezoid reduces to a triangular-velocity profile.

1.3 Crane Control

Payload oscillation originates from two sources. First, oscillation can be self-induced when a crane moves in response to commands. Such commands can originate from a human operator or a feedback loop. Second, the payload can be acted on by external disturbances, such as wind or a collision with an obstacle. Rahman provides an overview of open-loop and closed-loop crane control techniques developed during the 20^{th} century [2].

Closed-loop techniques use feedback of the payload state to generate crane movements that dampen payload oscillations. Unlike open-loop methods, these control strategies can correct oscillations originating from external disturbances. However, it can be challenging to accurately and reliably measure the payload state in non-ideal settings, such as in a cluttered manufacturing facility with dim lighting. Also, sensors for detecting the payload state can be expensive and unreliable.

Open-loop control strategies use knowledge about the dynamic system to diminish motion-induced payload oscillations. These methods fall into two categories: optimal control and input shaping [2]. The optimal control approach solves for an optimal trajectory that minimizes a cost function. Some methods seek a solution that minimizes payload oscillations, while others are only concerned with minimizing the travel time [2]. The optimized trajectory is subject to boundary conditions, including the start and end points, and must be resolved for each new move.

1.3.1 Input Shaping

Input shaping is a command filtering technique that reduces motion-induced oscillations by intelligently transforming the reference command. The transformation

involves convolving the reference command with an impulse sequence, called the input shaper. Input shapers can be designed for robustness to parameter variations and for suppressing multiple modes. Input shaping is implementable in real-time and can be used when humans generate the commands. This thesis uses input shaping to suppress multi-mode oscillations of a dual-hoist bridge crane.

To design an input shaper, a series of constraints are imposed on the impulse amplitudes, impulse times, and the vibration induced by the impulse sequence. Vibration constraints depend on knowledge about the natural frequencies and damping ratios of a system's modes. For an undamped, second-order system with an undamped natural frequency of ω_n and a damping ratio of ζ, the residual amplitude resulting from a sequence of impulses is described by [16]:

$$V(\omega_n, \zeta) = e^{-\zeta w_n t_n} \sqrt{[C(w_n, \zeta)]^2 + [S(w_n, \zeta)]^2} \tag{1.1}$$

where,

$$C(\omega_n, \zeta) = \sum_{i=1}^{n} A_i e^{\zeta w_n t_i} cos(w_d t_i) \tag{1.2}$$

and

$$S(\omega_n, \zeta) = \sum_{i=1}^{n} A_i e^{\zeta w_n t_i} sin(w_d t_i) \tag{1.3}$$

Here, V is non-dimensional and is called the Percent Residual Vibration (PRV). It is equivalent to the amplitude of residual vibration caused by the impulse sequence divided by the residual vibration amplitude caused by a single unity-magnitude impulse. The residual vibration amplitude can be reduced by choosing a vibration limit, V_{tol}, and placing a constraint on the maximum tolerable PRV:

$$e^{-\zeta w_n t_n} \sqrt{[C(w_n, \zeta)]^2 + [S(w_n, \zeta)]^2} \leq V_{tol} \tag{1.4}$$

To make the magnitude of the shaped command equal to that of the reference command, the impulse amplitudes can be constrained to sum to one:

$$\sum_{i=1}^{n} A_i = 1 \tag{1.5}$$

The first impulse time can be set to zero without loss of generality:

$$t_1 = 0 \tag{1.6}$$

The time locations of each impulse can be constrained to be in sequential order:

$$t_{i-1} < t_i \qquad i = 2, ..., n \tag{1.7}$$

An input shaper increases the rise time of the command by the final shaper impulse time, t_n. Therefore, the ideal solution minimizes t_n:

$$min(t_n) \tag{1.8}$$

Constraints (1.4)-(1.8) are common for all input shapers described in this thesis. Another constraint must be placed on the individual impulse amplitudes in order to find a solution. The following subsections describe different types of input shapers and their additional constraints.

1.3.2 Zero Vibration Shapers

By setting $V_{tol} = 0$ in (1.4), it is possible to obtain a shaper that theoretically achieves zero residual vibration at the modeling frequency. This is known as a Zero Vibration (ZV) shaper. The impulse amplitudes can be constrained to be greater than zero:

$$A_i > 0 \qquad i = 1, ..., n \tag{1.9}$$

This is known as a positive ZV shaper. The impulse sequence for a positive ZV shaper is a function of the damped period of oscillation (T_d) and damping ratio (ζ) [22, 16]:

$$\begin{bmatrix} A_i \\ t_i \end{bmatrix} = \begin{bmatrix} \frac{1}{K+1} & \frac{K}{K+1} \\ 0 & 0.5T_d \end{bmatrix}, \; i = 1, 2 \tag{1.10}$$

Table 1.3: UM-ZV Shaper for Damped Systems [19]

$$t_i = (M_0 + M_1\zeta + M_2\zeta^2 + M_3\zeta^3)\tau, \quad \tau = 2\pi/\omega$$

A_i	t_i	M_0	M_1	M_2	M_3
1	t_1	0	0	0	0
-1	t_2	0.16724	0.27242	0.20345	0
1	t_3	0.33323	0.00533	0.17914	0.20125

The damping ratio, ζ, scales the impulse amplitudes through the variable K given by:

$$K = e^{\left(\frac{-\zeta\pi}{\sqrt{1-\zeta^2}}\right)} \tag{1.11}$$

1.3.3 Unity-Magnitude Zero Vibration Shapers

Input shapers that produce faster motion than positive shapers can be designed if we allow negative impulses. One type of constraint that allows negative impulses, called a unity-magnitude (UM) constraint, requires all impulses to alternate between 1 and -1:

$$A_i = (-1)^{n+1} \qquad i = 1, ..., n \tag{1.12}$$

If the UM constraint is combined with the zero vibration constraint, then the resulting shaper is called a Unity-Magnitude Zero Vibration (UM-ZV) shaper. If $\zeta = 0$, then the UM-ZV impulse sequence is [19]:

$$\begin{bmatrix} A_i \\ t_i \end{bmatrix} = \begin{bmatrix} 1 & -1 & 1 \\ 0 & \frac{cos^{-1}(0.5)}{\omega_n} & \frac{cos^{-1}(-0.5)}{\omega_n} \end{bmatrix}, \; i = 1, 2, 3 \tag{1.13}$$

When ζ is nonzero, the impulse times are functions of ζ. No closed form solution exits. However, a third-order curve fit can be utilized to determine t_i to within 0.5% over the range $0 < \zeta < 0.3$ [19]. These curve fits are shown in Table 1.3.

1.3.4 Convolved Multi-Mode Shapers

Input shapers can be designed to suppress multiple frequencies. One way to create a multi-mode shaper is to design input shapers for each individual mode and then convolve them together [19]. For two shapers containing n impulses and m impulses, respectively, each new impulse is created by taking one impulse from each shaper and calculating the product of the impulse amplitudes and the sum of the impulse times. This is repeated for every combination of impulses between the two shapers, so the convolved shaper will have nxm impulses.

1.3.5 Specified Insensitivity Shapers

Specified Insensitivity (SI) shapers enable the designer to specify the required robustness for a particular application. This is accomplished by using a technique called frequency sampling [15], where selected frequencies are limited within the desired frequency suppression range. The number of suppressed frequencies is chosen by the designer. A numerical optimization function can be used to solve for an impulse sequence that satisfies the constraints.

1.3.6 Unity-Magnitude Maximum-Vibration Shapers

In his dissertation, Maleki provides a command shaper that is designed to increase the amplitude of vibration at a particular design frequency [12]. This is accomplished by enforcing a constraint that maximizes the PRV in (1.1) for ω_n and ζ. The Unity-Magnitude Maximum-Vibration Shaper is [12]:

$$\begin{bmatrix} A_i \\ t_i \end{bmatrix} = \begin{bmatrix} 1 & -1 & 1 \\ 0 & 0.5T_d & T_d \end{bmatrix}, \; i = 1, 2, 3 \tag{1.14}$$

where T_d is the damped period of oscillation.

1.4 System Identification of Dynamic Structures

Structural dynamics is concerned with understanding the response of engineering structures to dynamic loading. Dynamic forcing can cause vibration by exciting the modes of a system. Large oscillations can occur if the applied force is periodic and has a frequency close to the natural frequency of a mode. Typically, knowledge of structural dynamics is used to design safer structures that are able to withstand certain dynamic loading conditions.

Modal analysis is a process for identifying the natural frequencies, damping ratios, and mode shapes of a system. Modal analysis has been applied to aluminum beams [13], buildings [17], bridges [29], automobiles [23], and aircraft [24, 9]. He and Fu provide a detailed treatment of experimental and analytical modal analysis in [6]. In experimental modal analysis, energy is added to the system via a known force input which causes the structure to vibrate at frequencies that are contained in the frequency spectrum of the force input. The measured response and force input can then be used to create a frequency response function (FRF). The choice of the excitation force input determines the spectral energy content that is supplied to the system as well as the testing time required for calculating the FRF [5]. Common excitation waveforms are "harmonic excitation waveforms like discretely stepped sine, periodic excitation like multi-sine, transient excitation like sinusoidal sweeps or impact, and random excitation" [5].

Devices called shakers are used to apply sinusoidal excitations. In [5], the authors review the International Standard ISO-7626, which provides guidelines for experimentally determining a FRF from a sinusoidally swept input. The authors reference the recommendation given in [4] "to check that progress through the frequency range is sufficiently slow to check that the steady-state response conditions are attained before measurements are made." A sinusoidal sweep is classified as linear or logarithmic based on the algorithm used to transition throughout the frequency range of interest.

The maximum linear swept-sine rate a_{max} (Hz/min) recommended in ISO-7626 is [5]:

$$a_{max} < \frac{54 f_r^2}{Q^2} \tag{1.15}$$

where f_r is the estimated resonance frequency and $Q = 1/(2\zeta)$. The maximum logarithmic swept-sine rate S_{max} (oct/min) recommended in ISO-7626 is [5]:

$$S_{max} < \frac{77.6 f_r}{Q^2} \tag{1.16}$$

Based on these recommended maximum sweep rates, the swept-sine test can be time-consuming for a system containing a lightly-damped, low-frequency mode. For example, Figure 1.6 shows the time required to complete a sinusoidal sweep from 0.3 to 1.5 Hz using these maximum recommended sweep rates with f_r ranging from 0.3 to 1.5 Hz and ζ ranging from 0.01 to 0.1. Note that cranes typically have damping ratios very close to zero. Therefore, cranes represent a very time-consuming application for swept-sine identification methods.

Schwarz and Richardson describe impact testing as "a fast, convenient, and low cost way of finding the modes of machines and structures" [14]. Impact excitations, which can be imparted by a hammer strike, excite a spectrum of frequencies. The measured response can then be analyzed using Fast Fourier Transform (FFT) analyzers to determine the frequency response [14].

In control systems, many physical plants exhibit oscillatory behavior in response to control inputs. For cranes, payload oscillation occurs when the trolley moves in response to a velocity command. Also, a long, flexible robotic arm can vibrate when a motor torque is applied to move the end effector. A controls engineer may need to design a controller that limits oscillation in order to satisfy a performance requirement. In this situation, understanding how the system response is affected by the available control inputs, which are determined by the actuators, is critical for designing an effective controller.

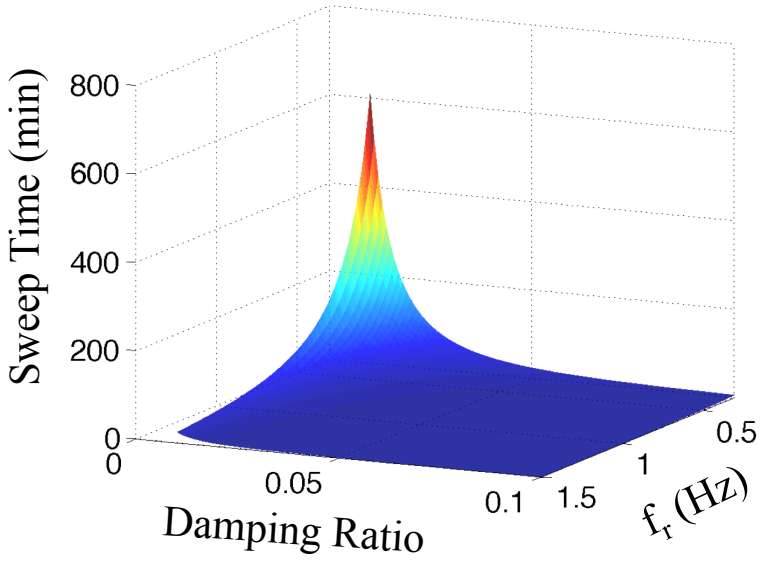

(a) Linear Sweep

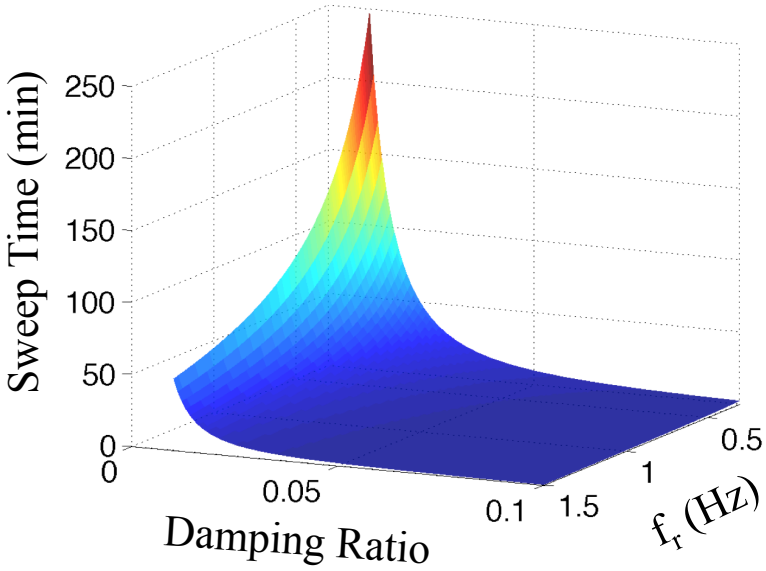

(b) Logarithmic Sweep

Figure 1.6: Time Required for 0.3-1.5 Hz Frequency Sweep

This thesis proposes a new system identification technique that uses the system's own actuators to examine modal characteristics of multi-mode systems. The frequency spectra of the reference commands are filtered by specially designed input shapers so that the frequencies and relative amplitude contributions of each mode can be determined. One advantage of this method is that the system's own actuators are utilized for system identification, and therefore, no additional excitation devices

are required. The results, which are obtained by analyzing dynamic responses originating from the system's own actuators, will also be representative of the system during normal operation.

1.5 Thesis Contributions

This thesis makes the following contributions:

1. An input shaper, called a Selective Mode Amplification (SMA) shaper, that amplifies one mode of a multi-mode system, while suppressing the others, in order to bring the small-amplitude mode to light.

2. A new system identification technique where input shaping is used to modify the frequency spectrum of the reference command in order to identify the frequencies and relative amplitude contributions of the individual modes in a multi-mode system.

3. An investigation of the dynamic response of a dual-hoist bridge crane moving distributed payloads using simulations and experiments.

4. An operator study where participants used a standard crane controller and an input-shaping controller to drive a dual-hoist bridge crane carrying triangular payloads through an obstacle in order to investigate human performance.

CHAPTER II

SELECTIVE MODE AMPLIFICATION SHAPERS

Each mode of a multi-mode system responds differently to any given reference command. It can be difficult to determine the frequency of a small-amplitude mode if a large-amplitude mode dominates the response to a given input. By modifying certain vibration constraints, it is possible to design an input shaper that amplifies one mode while suppressing the others. This process is effectively a type of band-pass filter. However, the passed frequencies are amplified as much as possible, rather than passed with a unity gain. This can be very beneficial for bringing the small-amplitude mode to light.

As an example multi-mode system that is challenging to identify, consider the dual-hoist bridge crane carrying a triangular payload that was shown in Figure 1.2a. The crane was moved in the bridge direction in a simulation. The system identification toolbox in MATLAB was used to determine the transfer functions of hook 1 (ϕ_1) and hook 2 (ϕ_2) in response to bridge motion. The simulation parameters were shown in Table 1.2.

The input used to drive the simulation was the acceleration profile required to accelerate the bridge at 1 m/s^2 to a maximum velocity of 0.33 m/s. The output was ϕ_1 for the hook 1 transfer function and ϕ_2 for the hook 2 transfer function, and the responses were simulated for 60 s. The first 6 seconds of the ϕ_1 output is shown in Figure 2.1. The function *tfest* was used for determining the transfer function from the input and output data. Six poles were specified as a parameter. The resulting transfer functions contained six complex poles with real parts close to zero. The frequencies were correctly identified as 0.38 Hz, 0.45 Hz, and 0.79 Hz.

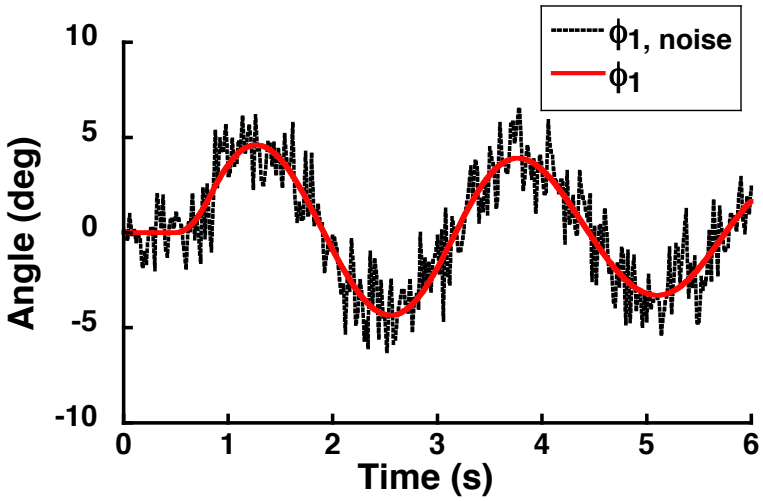

Figure 2.1: Hook 1 Response with White Gaussian Noise

The *wgn* function was used to generate white Gaussian noise. Each data point was divided by the maximum positive value contained in the data set and then multiplied by four. The resulting white noise data were added to ϕ_1 and ϕ_2 to simulate noisy hook angle measurements. The first 6 seconds of the noisy ϕ_1 output is also shown in Figure 2.1. The transfer function estimation process was repeated using the noisy ϕ_1 and ϕ_2 outputs. The 0.38 Hz and 0.45 Hz modes were correctly identified from the estimated hook 1 and hook 2 transfer functions. However, the highest frequency, located at 0.79 Hz, was misidentified as 1.44 Hz and 1.24 Hz, respectively, from the noisy ϕ_1 and ϕ_2 measurements. An input shaper designed to increase the small-amplitude mode could be useful for improving the estimation of the 0.79 Hz mode under noisy conditions.

The hook motions on the real crane are measured using downward-pointing cameras attached to the bottom of the trolleys. The cameras track markers placed on top of the hooks. If the camera cannot determine the position of the marker, then the camera measurement is set to zero. To investigate the effect that this camera measurement error can have on the determination of the oscillation frequencies, the ϕ_1 and ϕ_2 simulation responses (without white noise) were randomly set to zero 15

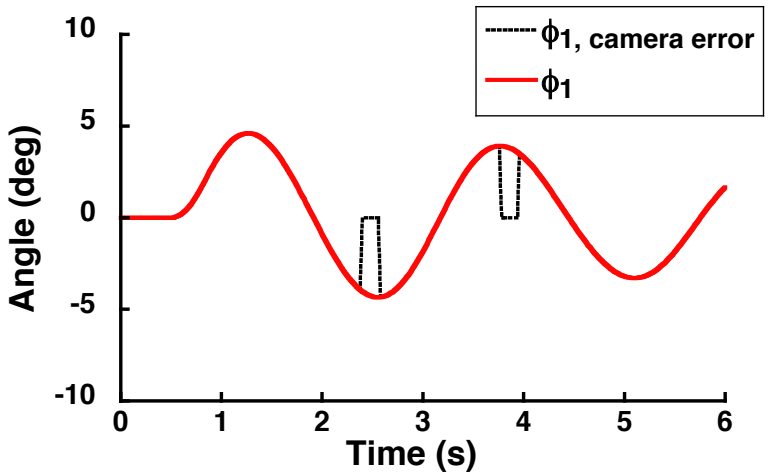

Figure 2.2: Hook 1 Response with Camera Measurement Error

times for a duration of 0.16-0.20 seconds each. The first six seconds of the altered and original ϕ_1 responses are shown in Figure 2.2. The transfer function estimation process was repeated using the altered ϕ_1 and ϕ_2 outputs. The 0.38 Hz and 0.45 Hz modes were correctly identified from the ϕ_1 transfer function, while the highest frequency mode at 0.79 Hz was misidentified as 1.28 Hz. From the ϕ_2 transfer function, the 0.38 Hz and 0.79 Hz modes were correctly identified, while the third mode was identified to be 1.15 Hz instead of 0.45 Hz. This example demonstrates how camera measurement error can affect the estimation of oscillation frequencies.

An input shaper designed to suppress a certain frequency will also generally suppress higher frequency modes. For example, a positive ZV shaper will suppress frequencies that are odd integer multiples of the design frequency. The vibration percentage, or PRV, for an impulse sequence can be calculated using (1.1) for a range of frequencies. A sensitivity curve shows the vibration percentage (y axis) as a function of frequency (x axis) for an impulse sequence. Figure 2.3 shows the sensitivity curve of a positive ZV shaper designed to suppress 0.37 Hz. If a system contained modes at 0.37 Hz and 1.11 Hz, then the positive ZV shaper would suppress both modes. As shown in Figure 2.3, a unity magnitude ZV (UM-ZV) shaper designed for 0.37 Hz

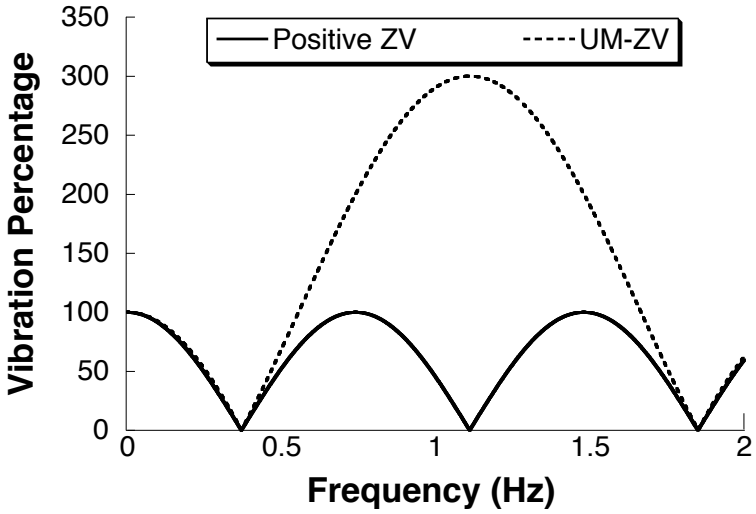

Figure 2.3: Sensitivity Curves of Shapers Designed for 0.37 Hz

will excite the 1.11 Hz mode to 300% of the unshaped value. For this reason, it is important to use an appropriate shaper if the goal is to suppress certain frequencies in order to bring a small-amplitude mode to light.

Negative shapers can suppress certain frequencies while amplifying other frequencies above that of positive shapers, as was demonstrated in Figure 2.3. This makes a negative shaper well suited for amplifying the response of one mode while suppressing other modes. Unity Magnitude amplitude constraints will be used for the Selective Mode Amplification (SMA) shaper that will be used to clarify a mode of interest:

$$A_i = (-1)^{i+1} \qquad i = 1, ..., n \tag{2.1}$$

To obtain a normalized result, the impulse amplitudes can be constrained to sum to one:

$$\sum_{i=1}^{n} A_i = 1 \tag{2.2}$$

The first impulse time can be set to zero without loss of generality:

$$t_1 = 0 \tag{2.3}$$

The time locations of each impulse must be in sequential order:

$$t_{i-1} < t_i \qquad i = 2, ..., n \tag{2.4}$$

Recall that (1.1) describes the residual amplitude resulting from an impulse sequence. A mode with a natural frequency ω_j and damping ratio ζ_j can be suppressed to below a specified limit, V_j, by imposing the constraint:

$$e^{-\zeta_j w_j t_n} \sqrt{[C(w_j, \zeta_j)]^2 + [S(w_j, \zeta_j)]^2} \leq V_j \qquad j = 1, ..., n \tag{2.5}$$

In this equation, V_j is the ratio of the shaped response to the unshaped response at ω_j. In order to amplify a particular frequency, ω_a, the vibration constraint is:

$$e^{-\zeta_a w_a t_n} \sqrt{[C(w_a, \zeta_a)]^2 + [S(w_a, \zeta_a)]^2} \geq V_a \tag{2.6}$$

where V_a is the residual amplitude limit that ω_a must exceed. The input shaper with the shortest rise time is desired, so the final impulse time t_n is the function to be minimized:

$$f_{min}(x) = t_n \tag{2.7}$$

The goal of the optimization problem is to find an impulse sequence that minimizes (2.7) subject to the constraints in (2.1)–(2.6).

2.1 Solution Approach

The SMA shaper can be derived numerically using a constrained nonlinear optimization program, such as $fmincon$ in MATLAB. However, the solution depends on an initial guess X_0 and the vibration constraints V_j and V_a. Poor choices for these parameters may result in the program failing to find a solution. A practical choice for X_0 can be obtained by combining smaller shapers that are designed for the individual

frequencies ω_j and ω_a. A ZV (1.10) or UM-ZV (1.13) shaper can be designed for each suppressed frequency ω_j, and a UM-MV shaper (1.14) can be designed for the mode to be amplified, at ω_a. These shapers can be convolved to generate a new shaper that can be used for X_0. Then, we know X_0 has $V_{j0} = 0$, and V_{a0} can be determined by finding the PRV from (1.1) with ω_a, ζ_a, and the impulse sequence X_0. These parameters can be used in the optimization function to find a SMA shaper, X, with less impulses and a shorter duration t_n. If X contains the desired frequency spectrum and duration, then the solution process is completed.

It is also possible to solve for a different shaper with the desired performance characteristics by modifying the constraints and resolving the optimization problem using X as the initial guess. For example, V_a can be increased by multiplying V_{a0} by a factor, k_a:

$$V_a = k_a V_{a0} \tag{2.8}$$

where $k_a > 1$. The tradeoff for an increased amplitude at ω_a is a longer shaper rise time. However, setting V_j to a small value, instead of zero, can decrease the rise time at the expense of a larger residual amplitude at ω_j.

2.2 SMA Shapers for Three-Mode Systems

A dual-hoist bridge crane with a triangular payload, such as the one shown in Figure 1.2a, has three modes. For the simulation parameters shown in Table 1.2, Figure 2.4 shows the undamped response of both hooks for a 0.4 m bridge motion. The hooks oscillate at 0.38 Hz, 0.45 Hz, and 0.79 Hz. The 0.38 Hz amplitude is much greater than that of the other two modes. Because the 0.38 Hz and 0.45 Hz frequencies are close, there is a beating effect between the two hooks. Note that the 0.79 Hz frequency is not readily apparent from this move. However, other motions might excite it to a problematic level.

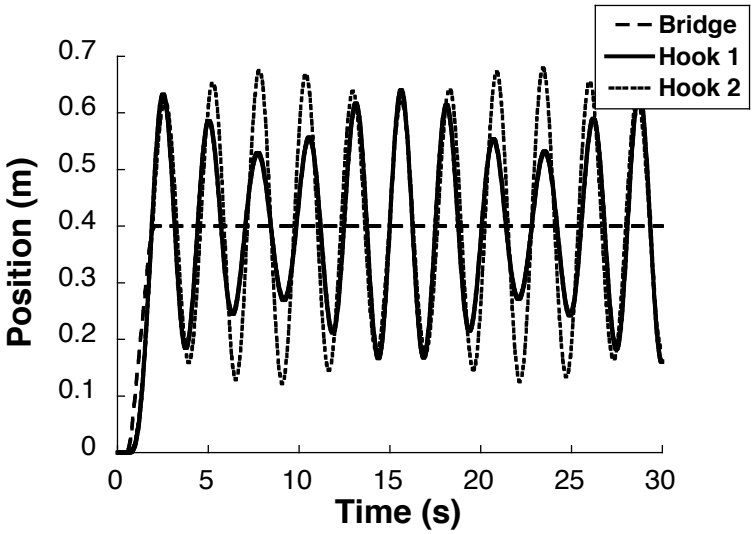

Figure 2.4: Hook Response for 0.4 m Bridge Motion

Table 2.1: SMA Shaper Design Parameters

Parameter	**Value**
Amplified Frequency, f_a	0.45 Hz
Minimum Vibration Percentage, V_a	65%
Suppressed Mode 1, f_1	0.38 Hz
Maximum Vibration Percentage, V_1	0
Suppressed Mode 2, f_2	0.79 Hz
Maximum Vibration Percentage, V_2	0

A two-mode Zero Vibration (ZV) shaper was created from the convolution of a 0.38 Hz ZV shaper and 0.79 Hz ZV shaper. Figure 2.5 shows the hook 1 response for a 0.4 m bridge move using the convolved ZV shaper. The peak-to-peak residual amplitude is approximately 0.02 m. A SMA shaper was designed to bring out the remaining 0.45 Hz mode by using the parameters in Table 2.1:

$$\begin{bmatrix} t(ms) \\ A \end{bmatrix} = \begin{bmatrix} 0 & 340 & 1040 & 1364 & 1689 & 2385 & 2727 \\ 1 & -1 & 1 & -1 & 1 & -1 & 1 \end{bmatrix} \tag{2.9}$$

The initial guess for the shaper-design optimization was the convolution of a 0.38 Hz

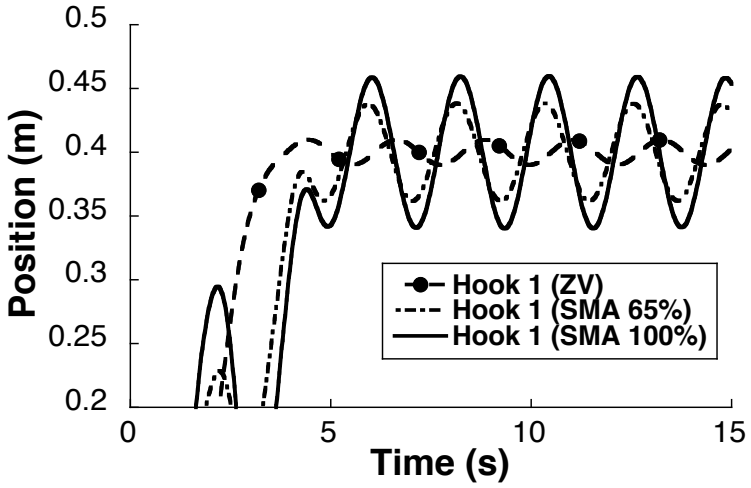

Figure 2.5: Shaped Hook 1 Response for 0.4 m Bridge Motion

UM-ZV shaper, 0.79 Hz UM-ZV shaper, and 0.45 Hz UM-MV shaper. The minimum vibration percentage, $V_a = 0.65$, of the amplified mode was calculated from (1.1) with $\omega_n = 0.45$, $\zeta = 0$, and the impulse sequence in (2.9). The hook 1 response resulting from a 0.4 m bridge move using the SMA shaper in (2.9) is also shown in Figure 2.5. The hook 1 residual amplitude is 0.08 m, which is four times greater than the convolved ZV-shaped response amplitude. The 0.45 Hz mode can be further amplified by increasing V_a. To illustrate this, a different SMA shaper was solved for by using (2.9) as the initial guess and increasing V_a to 100%:

$$\begin{bmatrix} t(ms) \\ A \end{bmatrix} = \begin{bmatrix} 0 & 481 & 1143 & 1455 & 1767 & 2431 & 2911 \\ 1 & -1 & 1 & -1 & 1 & -1 & 1 \end{bmatrix} \tag{2.10}$$

The peak-to-peak residual amplitude increases to 0.12 m when (2.10) is used to complete a 0.4 m bridge move, as shown in Figure 2.5.

This chapter presented a new type of input shaper, called a Selective Mode Amplification (SMA) shaper, that can be used to bring a small-amplitude mode to light. Chapter 3 presents a new system identification method, called Input-Shaped System Identification, that uses SMA shapers to distinguish the frequencies and relative

amplitudes of the modes in a multi-mode system.

CHAPTER III

INPUT-SHAPED SYSTEM IDENTIFICATION

This thesis proposes a new system identification technique, called Input-Shaped System Identification, that uses the system's own actuators to examine modal characteristics of multi-mode systems. The frequency spectra of the reference commands are filtered by specially designed input shapers so that the frequencies and relative amplitude contributions of each mode can be determined. One advantage of this method is that the system's own actuators are utilized for system identification, and therefore, no additional excitation devices are required. The results, which are obtained by analyzing dynamic responses originating from the system's own actuators, will also be representative of the system during normal operation. Input-Shaped System Identification is especially useful for an engineer who is designing input shapers for lightly-damped systems. For systems with low damping, zero damping can be assumed for the input shaper design with a minimal decrease in performance. Furthermore, this method can be used to improve the frequency estimation from noisy measurements.

In order to control a flexible system effectively, it is important to understand how the system will respond to a specified input. This can be accomplished by applying an input to the system and measuring the response. The impulse response of a single-mode system is shown in Figure 3.1. The oscillation amplitude and frequency of the single mode can be easily determined from the time response.

The impulse response of a three-mode system is also shown in Figure 3.1. The total response is a combination of the three individual modes. The total response can be represented as a combination of these three individual modes. However, determining

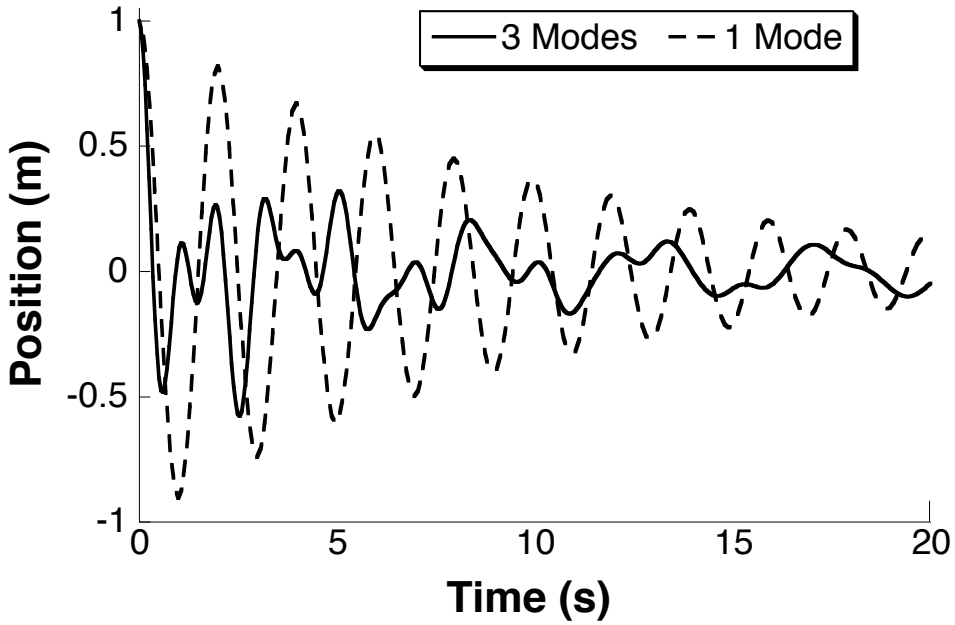

Figure 3.1: Impulse Response of Two Systems

the three components is not easy, especially when one mode dominates, or there is significant measurement noise. Knowledge about the contributions (oscillation amplitudes) of each mode to the total response can be used to design a controller that limits the total oscillation amplitude within a tolerable level. For example, an input shaper can be designed to suppress the oscillation amplitudes of each mode to within an acceptable level, resulting in an acceptable level of vibration for the total response.

As an example multi-mode system that is challenging to identify, consider the dual-hoist bridge crane carrying a triangular payload that was shown in Figure 1.2a. The payload response to bridge motion contains three modes. If the bridge is moved, then the frequencies can be determined by performing a Fast Fourier Transform (FFT) of the ϕ_1 and ϕ_2 time response data. Some systems may have additional modes that are not clearly identified by the FFT. To check for additional modes, the bridge can be moved with an input shaper designed to suppress the modes that are already known.

As was demonstrated in Figure 2.3, an input shaper designed to suppress a certain

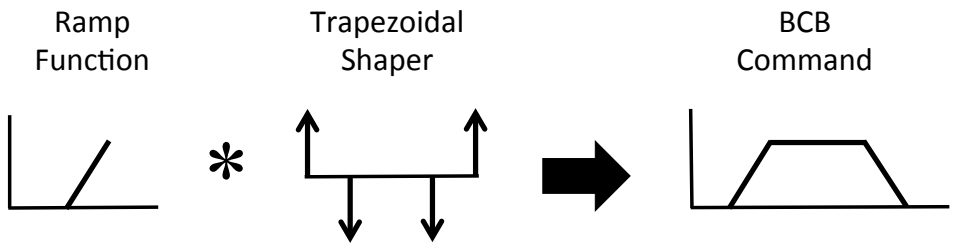

Figure 3.2: Bang-Coast-Bang Command Construction

frequency will also generally suppress higher frequency modes. For this reason, it is important to use an appropriate shaper if the goal is to suppress certain modes in order to distinguish other modes.

The frequencies of a multi-mode system may change as a function of the system parameters. For example, the mode frequencies vary as the triangular payload mass is increased for the dual-hoist bridge crane configuration that was shown in Figure 1.2a. Knowledge of how the modes vary as the system parameters are changed can be used to design an oscillation-reducing controller that is robust to parameter variations. However, the reference command determines the frequency content of the energy for changing the system state, which also excites the modes. Therefore, it is important to understand how the reference command affects the system response.

3.1 Bang-Coast-Bang Command

The dual-hoist bridge crane is programmed to generate trapezoidal bang-coast-bang (BCB) trajectories in response to operator-issued commands from a human machine interface (HMI). The generated BCB command depends on the acceleration (a), maximum velocity (v_{max}), and the duration of the operator-issued command. Alternatively, the BCB trajectory can be derived from the desired move distance, x_d, instead of the command duration. The BCB command can be described as the convolution of a series of four impulses, referred to as the *trapezoidal shaper*, with a ramp function.

This BCB command construction process is illustrated in Figure 3.2.

For $v_{max} = 1\ m/s$, $a = 1\ m/s^2$, and $x_d = 1\ m$, the trapezoidal shaper is:

$$\begin{bmatrix} A_i \\ t_i \end{bmatrix} = \begin{bmatrix} 1 & -1 & -1 & 1 \\ 0 & 0.330 & 3.030 & 3.360 \end{bmatrix} \tag{3.1}$$

If the move distance is change to $x_d = 1.2\ m$, then the trapezoidal shaper is:

$$\begin{bmatrix} A_i \\ t_i \end{bmatrix} = \begin{bmatrix} 1 & -1 & -1 & 1 \\ 0 & 0.330 & 3.636 & 3.966 \end{bmatrix} \tag{3.2}$$

Finally, for $x_d = 1.4\ m$, the trapezoidal shaper is:

$$\begin{bmatrix} A_i \\ t_i \end{bmatrix} = \begin{bmatrix} 1 & -1 & -1 & 1 \\ 0 & 0.330 & 4.242 & 4.572 \end{bmatrix} \tag{3.3}$$

Figure 3.3 shows the sensitivity curves for the trapezoidal shapers in (3.1)–(3.3). Each curve has a unique frequency spectrum with different peaks and troughs. However, when the peaks are observed together, they resemble another peak-trough profile that stretches from 0 to 3 Hz.

The first and second impulses from the BCB commands in (3.1)–(3.3) are identical. Figure 3.3 also shows the sensitivity curve, labeled 1/2 BCB, for these first two impulses:

$$\begin{bmatrix} A_i \\ t_i \end{bmatrix} = \begin{bmatrix} 1 & -1 \\ 0 & 0.330 \end{bmatrix} \tag{3.4}$$

This sensitivity curve has the same shape, only with a smaller vibration percentage, as the profile created by the peaks from the (3.1)–(3.3) sensitivity curves. This is because the final two impulses in (3.1)–(3.3), which have the same elapsed time between them

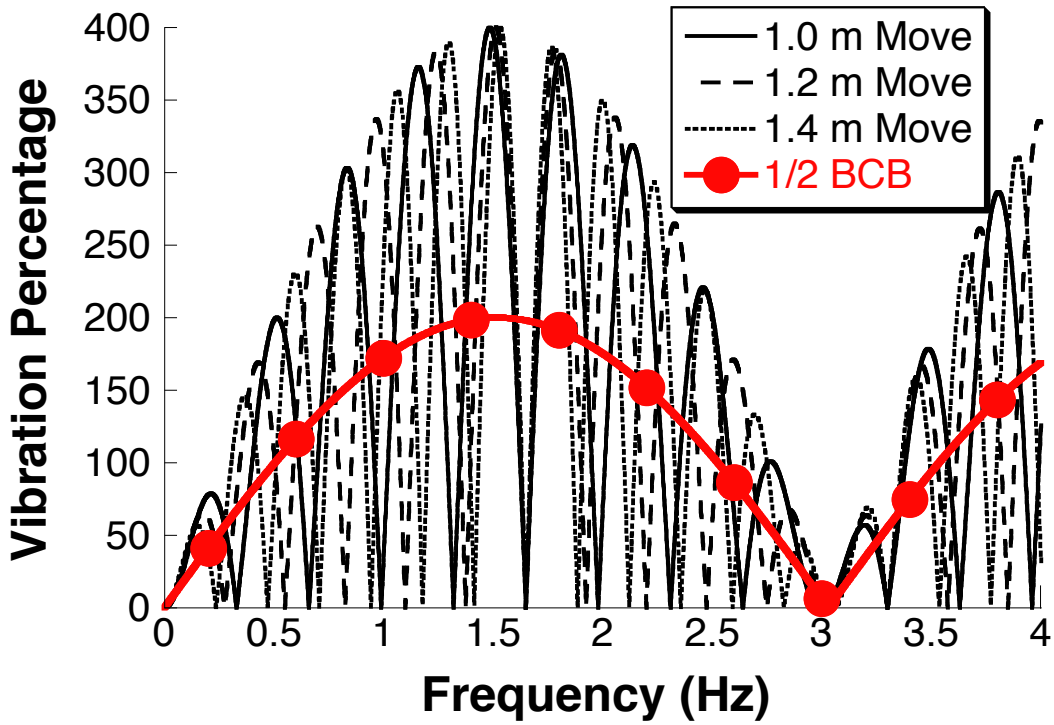

Figure 3.3: Trapezoidal Shaper Sensitivity Curve

as the first two impulses, either amplify or attenuate the response excited by the first two impulses. The maximum vibration percentage in the 1/2 BCB curve is 200%, and if the final two impulses in the full BCB command are applied at the proper time, then the maximum vibration percentage of 400% will occur at a certain frequency.

3.2 Total Shaper

The *total shaper* describes all of the impulses that are used to control the system in response to a reference command. For systems that are controlled with BCB commands, the *total shaper* is the same as the *trapezoidal shaper* in the absence of command shaping. When input shaping is used, the *total shaper* is the impulse sequence created by the convolution of the *trapezoidal shaper* and the input-shaper impulse sequences, as demonstrated in Figure 3.4.

An oscillatory response may result if a particular *total shaper* is used to move a flexible system. If the response contains a single mode at a frequency of ω_a, then

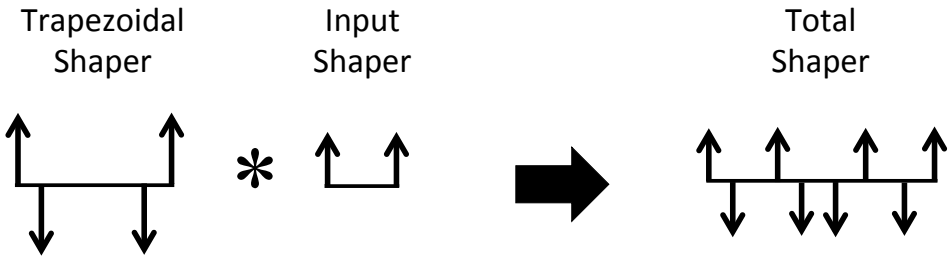

Figure 3.4: Total Shaper Impulse Sequence

the PRV at ω_a can be determined by plugging ω_a, ζ_a, and the total shaper impulse sequence into the PRV equation in (1.1). The resultant is called the *total shaper factor*. Dividing the residual vibration amplitude by the *total shaper factor* scales the amplitude so that it represents the amplitude of ω_a which originates from a single impulse.

3.3 Method for Input-Shaped System Identification

This section presents a method for determining the frequencies and relative amplitudes of each mode of a multi-mode system for different system configurations. The Input-Shaped System Identification method consists of two parts. The first part uses input shaping to modify the frequency spectrum of the reference command for discovering the modal frequencies. The second part uses SMA shapers to suppress all but one mode so that the measured response is primarily composed of the single mode of interest. Then, the relative amplitude of each mode that results from a single impulse can be determined.

3.3.1 Frequency Identification Process

The frequency identification process uses a FFT of the measured response to determine the modal frequencies after the system has been moved with it's own actuators. Then, input shapers are designed to suppress the discovered modes in order to increase the signal-to-noise ratio of the measured response for the identification of additional

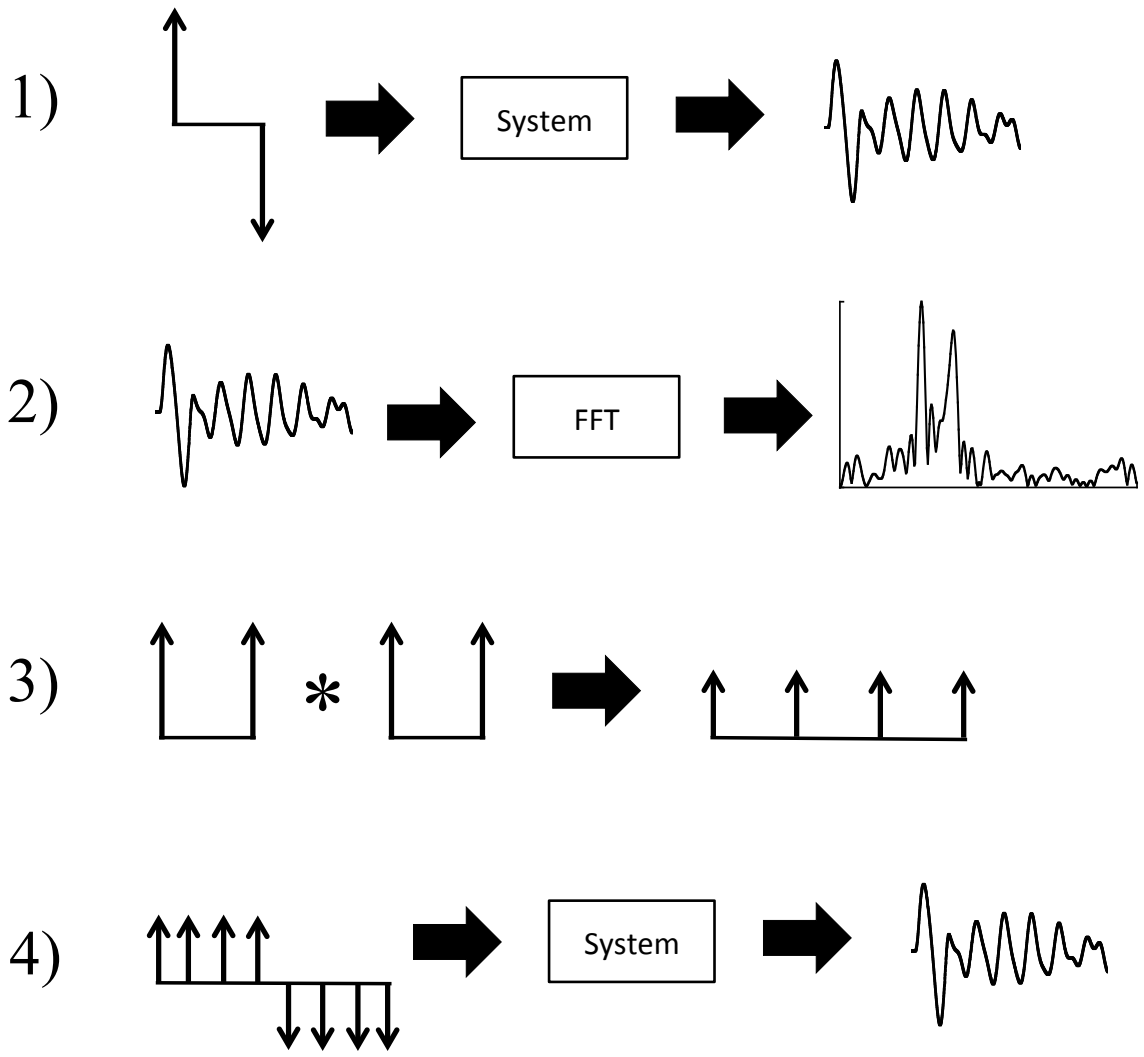

Figure 3.5: Frequency Identification Process

modes.

The proposed frequency identification process, illustrated in Figure 3.5, is accomplished with the following process:

1. Apply the first two impulses of the trapezoidal shaper, and measure the oscillation response while the system is in motion. If it is not possible to appropriately measure the response while the system is in motion, then measure the response after a series of random movements along the same axis in order to reduce the

probability of suppressing one of the modes.

2. Use a FFT to determine the frequency spectrum of the measured time response.

3. Design an input shaper to suppress the modes that are discovered. It is best to use a shaper that has low robustness, such as a ZV shaper, UM-ZV shaper, or SI shaper, to decrease the chance that higher modes will be suppressed.

4. Use the input shaper to repeat the move completed in step 1, and measure the oscillation response

5. Repeat steps 2-4 until no other frequencies are found.

3.3.2 Amplitude Identification Process

The amplitude identification process uses SMA shapers designed to suppress all but one mode so that the measured response is primarily composed of the single mode of interest. Then, the amplitude of the remaining mode can be easily determined from the time response. A SMA shaper can be designed for each mode. By systematically measuring the SMA-shaped responses, the relative amplitude contribution of each mode can be identified.

The flowchart in Figure 3.6 shows a process for experimentally determining the relative amplitude of each mode in the response of a multi-mode system. The elements in this flowchart will be explained, and then the entire process will be summarized.

If the modal frequencies are known for a given configuration of system parameters, then it is possible to design a SMA shaper that suppresses, to a very low level, all but one mode that has a natural frequency of ω_a. Then, the system response can be measured when the reference command is shaped by the SMA shaper in order to determine the targeted mode's residual vibration amplitude. The *total shaper* is the convolution of the reference command and SMA shaper impulse sequences. The PRV at the mode of interest, called the *total shaper factor*, can be determined by

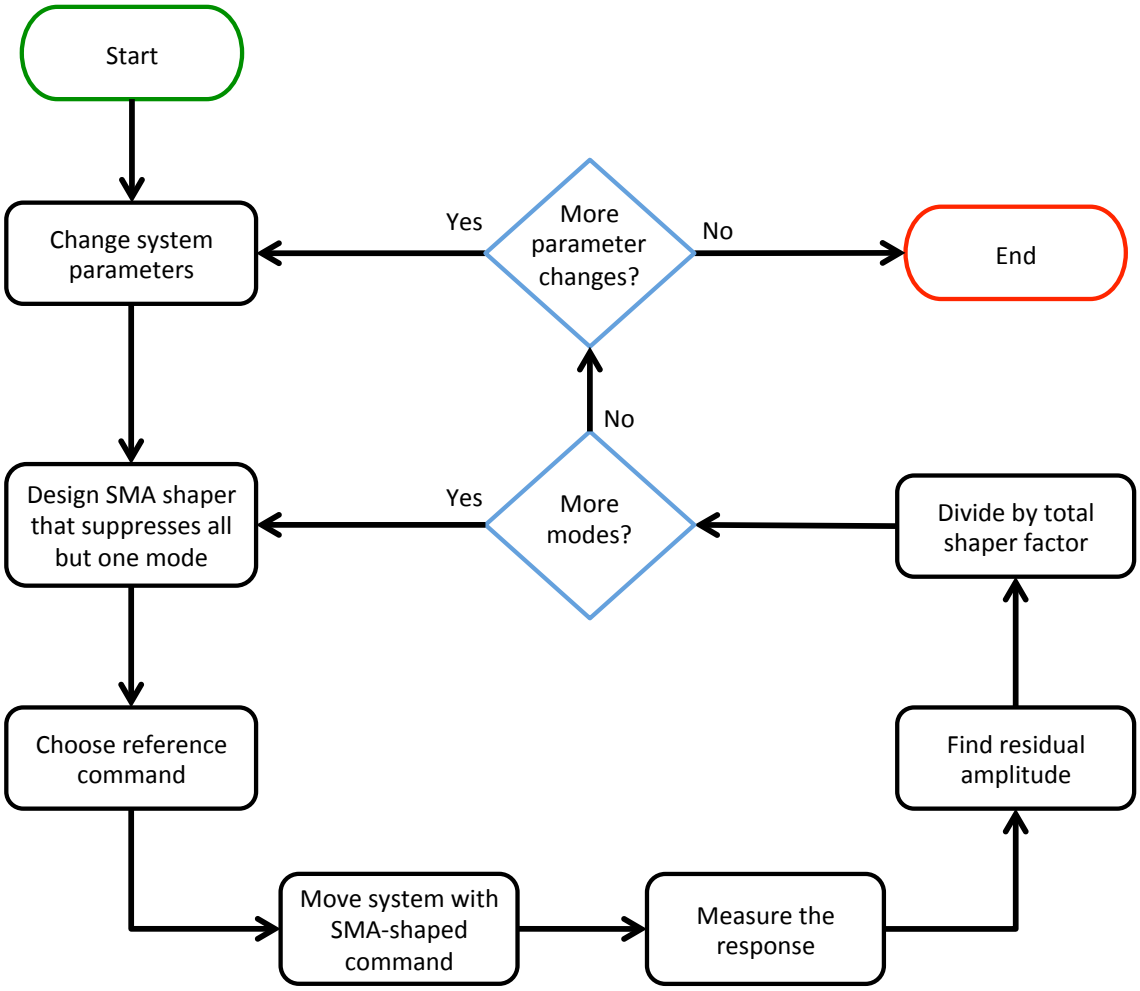

Figure 3.6: Amplitude Identification Flowchart

plugging ω_a, ζ_a, and the total shaper impulse sequence into the PRV equation in (1.1). Dividing the residual vibration amplitude by the *total shaper factor* scales the amplitude so that it represents the amplitude of ω_a which originates from a single impulse. This can be repeated for each mode so that the relative amplitude of each mode that originates from a single impulse can be identified. Then, the process can be repeated for different system configurations to determine the frequency and relative amplitude for each mode as the system parameters are changed.

It is important to use consistent reference commands when discovering the amplitude of each mode so that the amplitudes can be directly compared at the completion

of the amplitude identification process. For systems that use BCB commands, the acceleration, a, should be kept constant because it affects the magnitude of the impulses that act on the system. The other parameters affecting the shape of the reference command will then be appropriately accounted for by dividing the residual vibration amplitude by the *total shaper factor*.

The shape of the reference command can be selected based on the mode frequencies and v_{max}. For example, if the mode of interest has a period that is less than the elapsed time between the first and second impulses of the trapezoidal shaper, then the residual vibration amplitude can be measured after only one impulse. The reference command would be the single impulse. However, if the period is longer than the elapsed time between the first two impulses, then the residual vibration amplitude can be measured after the system reaches coasting velocity. This reference command would be the first two impulses of the trapezoidal shaper.

If it is not possible to measure the residual vibration amplitude while the system is in motion, then the complete trapezoidal shaper can be used as the reference command. However, the selected move distance can result in cancellation of the mode of interest. Therefore, a move distance should be selected that results in a suitable residual vibration amplitude, in comparison to what occurs after the first two impulses, to improve the accuracy of the amplitude identification process.

The amplitude identification process is summarized as follows:

1. For the current system configuration, design an input shaper, such as an SMA shaper, that suppresses all modes except for one.

2. Measure the response after the system has been moved with the SMA-shaped reference command.

3. Determine the residual amplitude of the measured response.

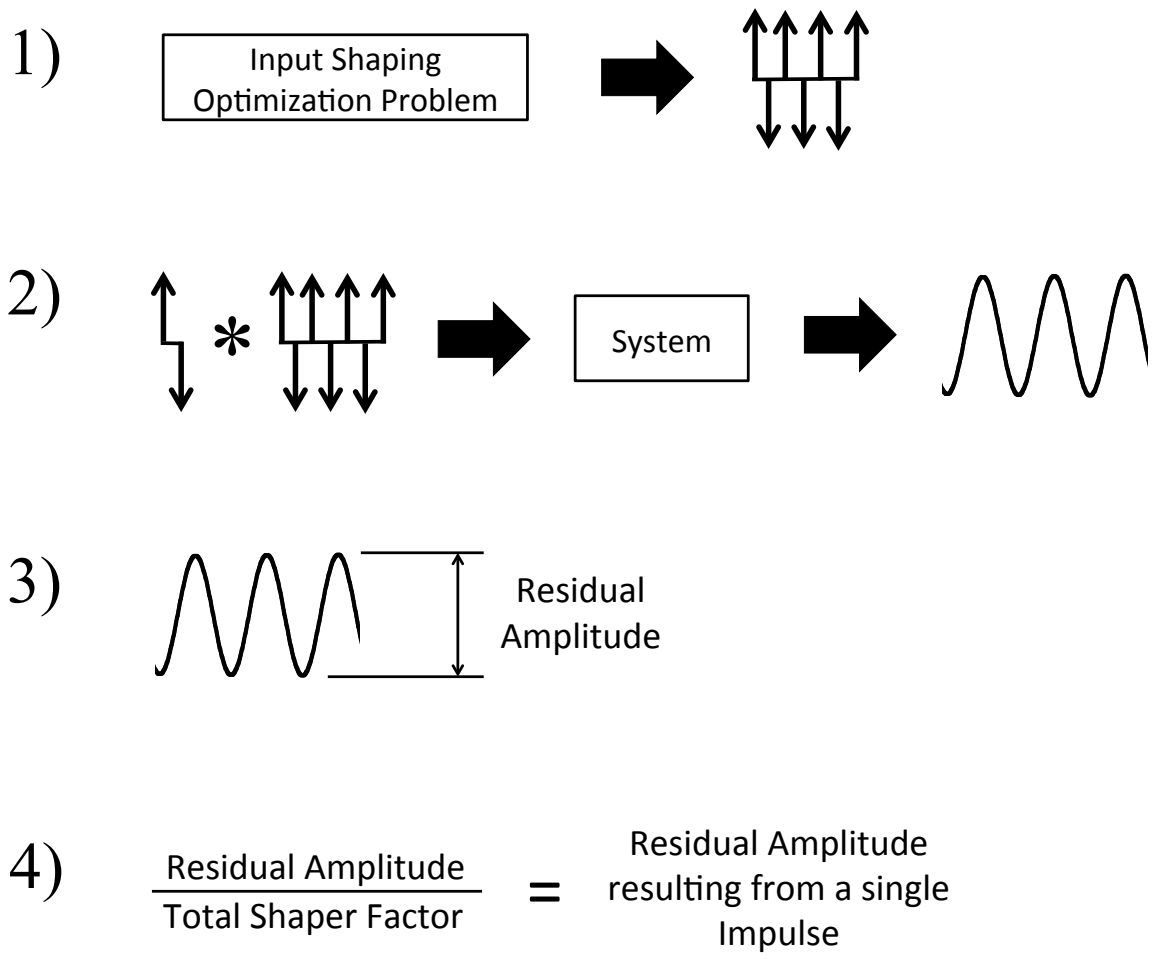

Figure 3.7: Amplitude Identification Process

4. Divide the residual amplitude by the *total shaper factor* to determine the vibration amplitude that results from a single impulse.

5. Repeat steps 1-4 for each additional mode.

6. Repeat steps 1-5 for each additional system configuration.

This chapter presented a new system identification method, called Input-Shaped System Identification, that uses input shaping to distinguish the frequencies and relative amplitudes of the modes in a multi-mode system. In the frequency identification process, input shapers are used to increase the signal-to-noise ratio of the measured

response for determining the modal frequencies. In the amplitude identification process, SMA shapers are designed to suppress all but one mode so that the SMA-shaped response is primarily composed of the single mode of interest. Then, the amplitude of the remaining mode can be easily determined from the time response. By systematically measuring the SMA-shaped responses for each mode and dividing the residual amplitude by the *total shaper factor*, the relative amplitude of each mode that results from a single impulse can be determined.

Chapter 4 investigates the dynamic response of a dual-hoist bridge crane moving distributed payloads using simulations and experiments. The Input-Shaped System Identification method is used to characterize the modes as a function of certain system configuration parameters.

CHAPTER IV

DYNAMICS AND CONTROL OF DUAL-HOIST BRIDGE CRANES MOVING DISTRIBUTED PAYLOADS

This chapter investigates the dynamic response of a dual-hoist bridge crane moving distributed payloads using simulations and experiments. The mathematical model used for simulations described in Section 1.2.2 was obtained using the commercial dynamics package MotionGenesis [1]. The computer code is listed in Appendix A. The results from the numerical model were validated with experiments performed on a dual-hoist bridge crane described in Section 1.2.1 located in the Hibay of the Manufacturing Research Center (MaRC) at Georgia Tech.

Most crane models ignore the inertial effects of the payload by lumping the hook and payload together as a point mass [2]. However, as the payload size increases, the rotational inertia effects of the payload can be evident in the oscillatory response of the system. This chapter investigates a particular kind of distributed payload that has a triangular shape, as was shown in Figure 1.2a. The triangular geometry was chosen because it is simple to model and construct, while capturing the important dynamic characteristics of generalized distributed payloads.

4.1 Dynamic Behavior and Control

The dual-hoist bridge crane has several degrees of freedom, so it can be operated in a large variety of configurations. The dynamic response of the system depends strongly on the input parameters and the system configuration. This section investigates the effect of the system configuration and explores the response to various inputs. Table 1.2 showed the nominal parameters used to simulate the system.

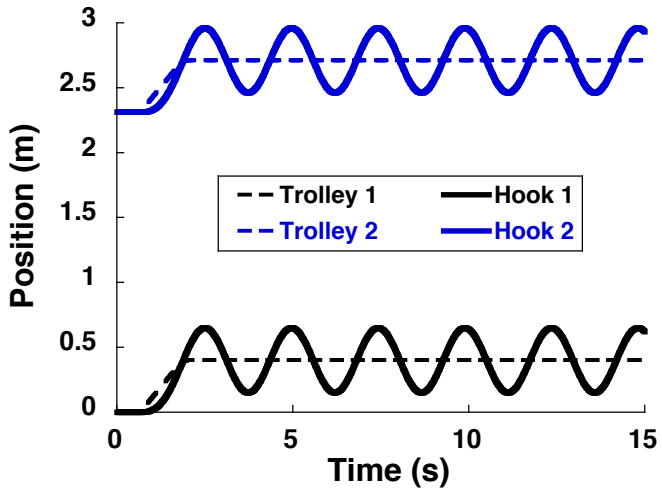

Figure 4.1: Response Induced by Simultaneous 0.4 m Motions by Both Trollies

4.1.1 Trolley Motion

Figure 4.1 shows the oscillation of both hooks induced by a 0.4 m motion in the trolley direction. Both trolleys were moved simultaneously to keep the separation distance constant. In this configuration, both hooks are initially hanging directly below the cable attachment points, and the initial rotation angles of the payload (β, γ, and ψ), and of the hooks (θ_1, θ_2, ϕ_1, and ϕ_2) are all zero. When the crane stops, both hooks oscillate about the trolley positions with a peak-to-peak amplitude of approximately 50 cm. This configuration is similar to a planar, single-hoist crane. Therefore, the response is a simple one-mode oscillation.

Figure 4.2 shows the residual swing amplitude of hook 2 induced by trolley moves ranging from 0.1 m to 2.0 m. Because motion in the trolley direction induces a single-mode swing, a simple input shaper, such as a Zero Vibration (ZV) shaper, can be used to reduce the swing. The swing amplitudes induced by the ZV-shaped commands (the damping ratio was assumed to be zero) are also shown in Figure 4.2. The ZV shaper reduced the residual swing to near zero over the entire range of move distances.

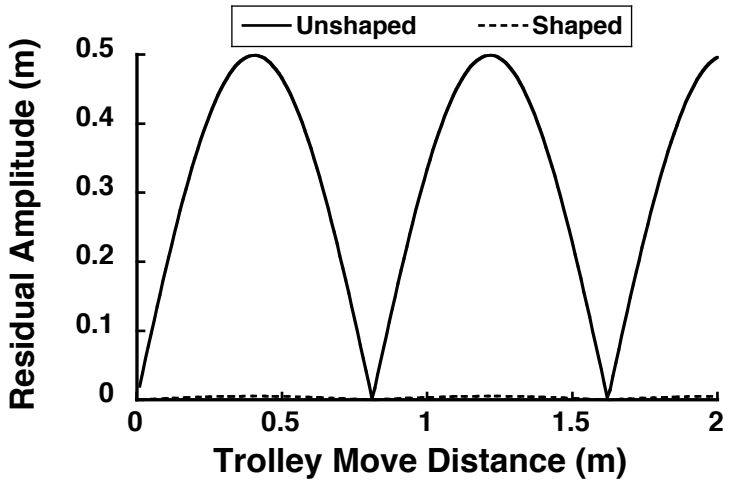

Figure 4.2: Residual Amplitude for Shaped and Unshaped Trolley Motions

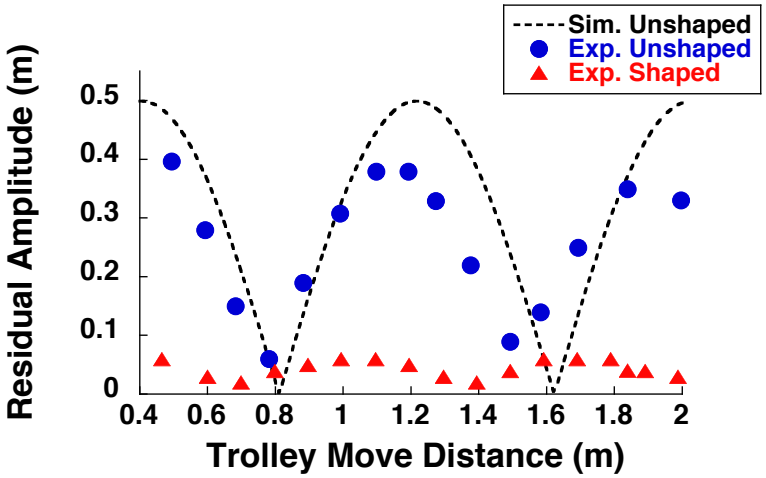

Figure 4.3: Residual Amplitude for Hook 2

The dual-hoist bridge crane was used to collect experimental data for comparison with the simulation data. The trolleys were simultaneously moved for distances ranging between 0.4 m and 2.0 m. Figure 4.3 shows the resulting peak-to-peak residual oscillation amplitude for Hook 2. The figure also shows the simulation results that were previously shown in Figure 4.2. The experimental and simulation results follow very similar trends. The residual amplitude curves contain peaks and troughs as the move distance varies. The experimental peaks, however, get smaller as the distance gets larger. This is due to the damping effect present in the real crane that

is not modeled in the simulation. Figure 4.3 also shows the residual swing induced by ZV-shaped commands for the same range of trolley motions. The ZV shaper was designed for a frequency of 0.41 Hz (which is approximately the frequency of a simple pendulum with a 1.5 m cable length). The ZV shaper reduced the residual oscillation by an average of approximately 77% over the entire range of move distances.

4.1.2 Bridge Motion

To investigate non-planar dynamics, the dual-hoist bridge crane was moved in the bridge direction. Note that the trolleys cannot move independently in the bridge direction. Figure 4.4 shows the hook responses for a 0.9 m bridge motion for the parameters that were shown in Table 1.2. Both hooks oscillate relative to the bridge position.

Three modes are present in the oscillation of the hooks, and the 0.9 m bridge move distance was chosen because all three modes are visible in the hook responses. The lowest-frequency "swing" mode corresponds to the payload swinging like a pendulum from the trolley hoists. The middle-frequency "twist" mode corresponds to the twisting motion that was shown in Figure 1.5b. The highest-frequency "roll" mode corresponds to the rolling motion that was shown in Figure 1.5c.

A FFT of the ϕ_1 and ϕ_2 time responses revealed oscillation frequencies of approximately 0.38 Hz, 0.45 Hz, and 0.79 Hz. These frequencies correspond to the swing, twist, and roll modes, respectively. Because 0.38 Hz and 0.45 Hz are close, there is a beating effect between the two hooks in Figure 4.4.

The dynamics were simulated for 60 s. During that time, hook 1 oscillates with a maximum peak-to-peak amplitude of approximately 14 cm, and hook 2 oscillates with a maximum peak-to-peak amplitude of approximately 13 cm.

For the bridge motion shown in Figure 4.4, the payload twist angle (γ) is no longer zero as it was for the planar motion induced by only trolley motion. Figure 4.5 shows

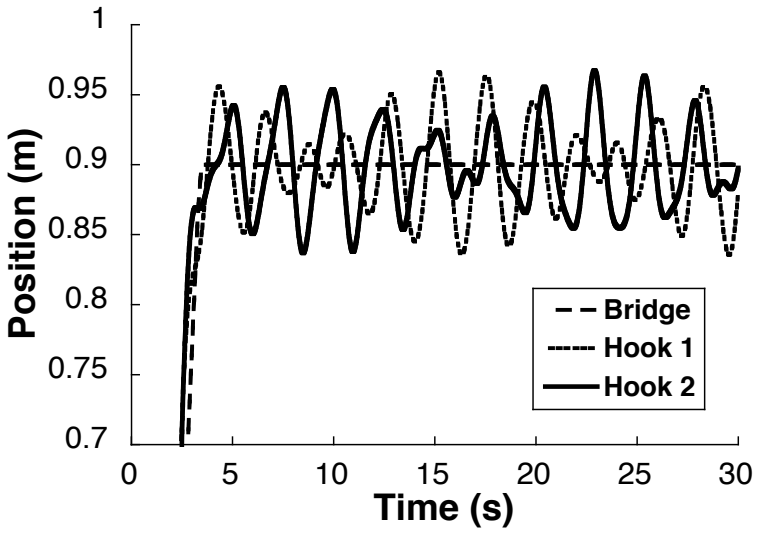

Figure 4.4: Response Induced by 0.9 m Bridge Motion

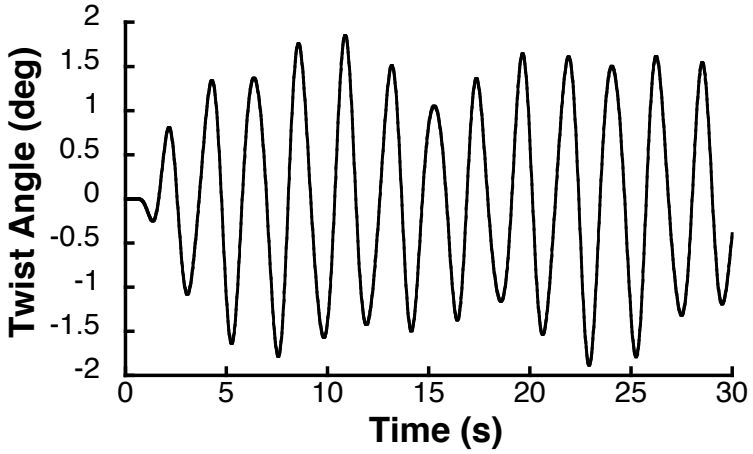

Figure 4.5: Response Induced by 0.9 m Bridge Motion

how the γ angle changes due to the 0.9 m move. The payload twist also exhibits a multi-mode oscillation.

The oscillation frequencies of the two hooks (if treated as independent of each other) are determined by the suspension cable length, but the hooks are attached together via the triangular payload. This configuration, the triangular payload geometry, and the non-planar motion result in the multi-mode oscillation shown in Figure 4.6.

Figure 4.7 shows the residual swing amplitude induced by bridge moves between

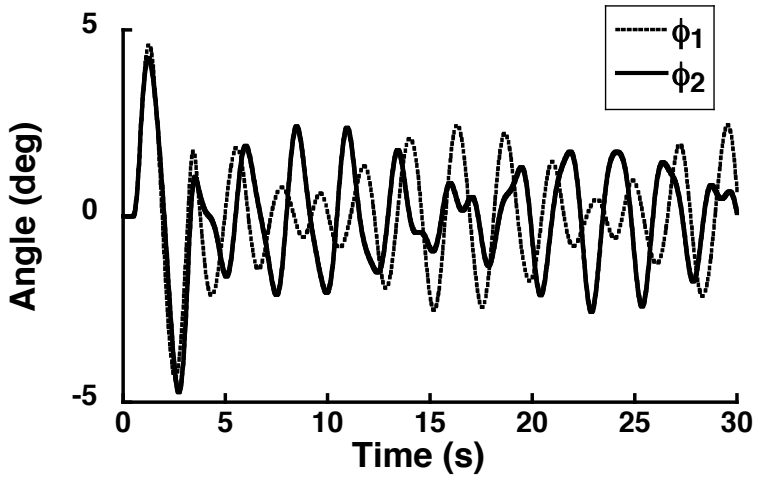

Figure 4.6: Response Induced by 0.9 m Bridge Motion

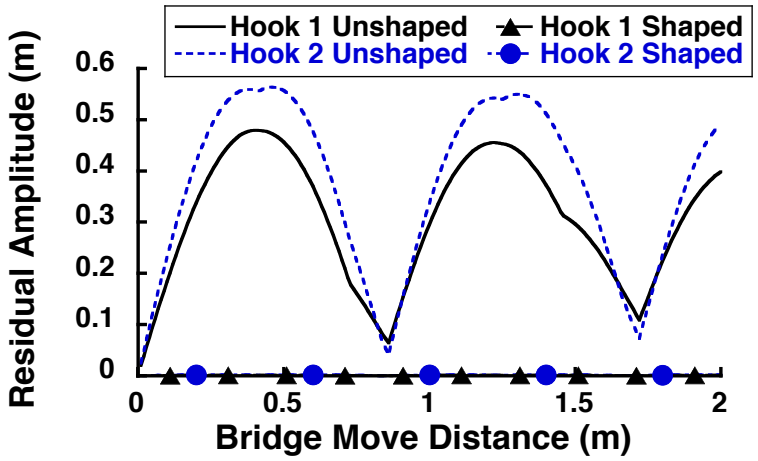

Figure 4.7: Residual Amplitude for Unshaped and Shaped Bridge Motions

0.1 m to 2.0 m. To reduce the hook swing induced by bridge motions, a three-mode ZV shaper was designed for 0.38 Hz, 0.45 Hz, and 0.79 Hz (the damping ratio was assumed to be zero). The swing amplitudes induced by the shaped commands are also shown in Figure 4.7. The three-mode ZV shaper reduced the residual oscillation of hook 1 and hook 2 to near-zero over the entire range of move distances.

Next, the dual-hoist bridge crane was used to experimentally determine the residual oscillation amplitude resulting from bridge motions. Figure 4.8 shows the residual amplitude in response to bridge motion for a 7 kg triangular payload. The curves

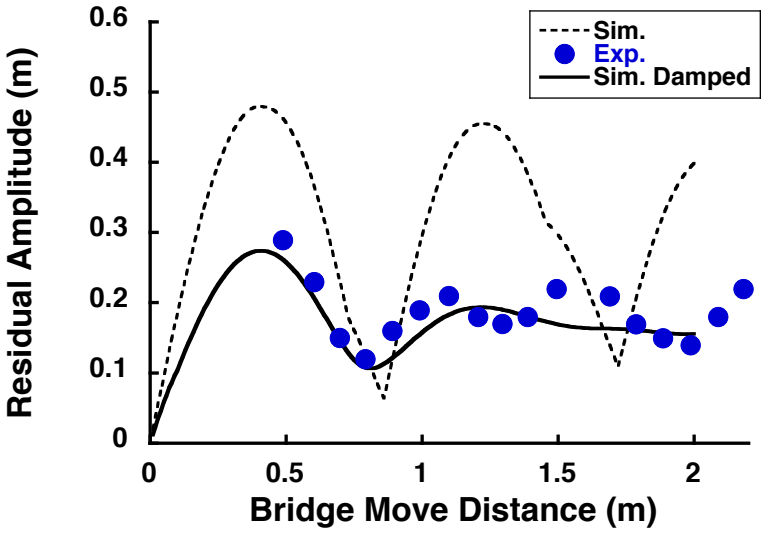

(a) Hook 1

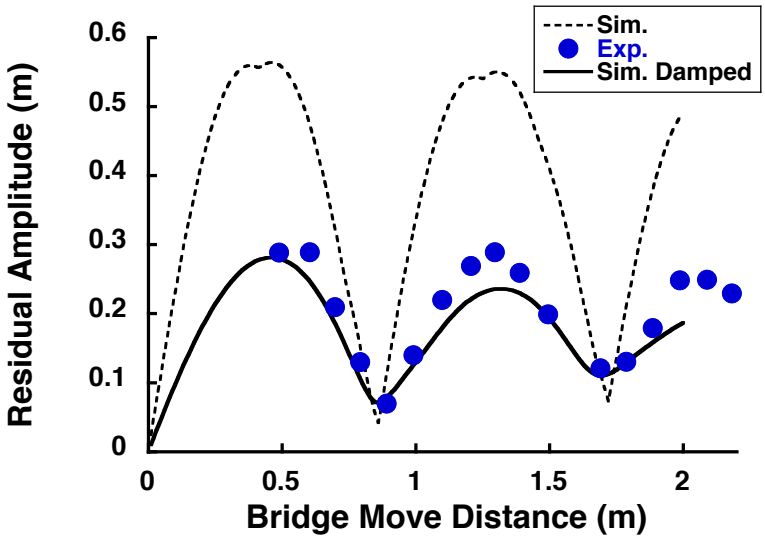

(b) Hook 2

Figure 4.8: Residual Amplitude Plot for a 7 kg Payload Mass

generated from the simulation in Figure 4.7 are also shown. The peaks of the experimental curves are much lower than the simulation curves because damping forces were not modeled in the simulation. Also, the hook 1 experimental curve has a different shape compared to the simulation curve.

New parameters were added to the simulation to account for damping between the suspension cables and the trolleys (B_1 and B_2) and the wind resistance that acts on the center of mass of the payload (B_p). Wind resistance has a greater impact on the

Table 4.1: Dual-Hoist Crane Simulation Damping Parameters

Parameter	Value
B_1	5 Ns/rad
B_2	1 Ns/rad
B_p	7 Ns/m

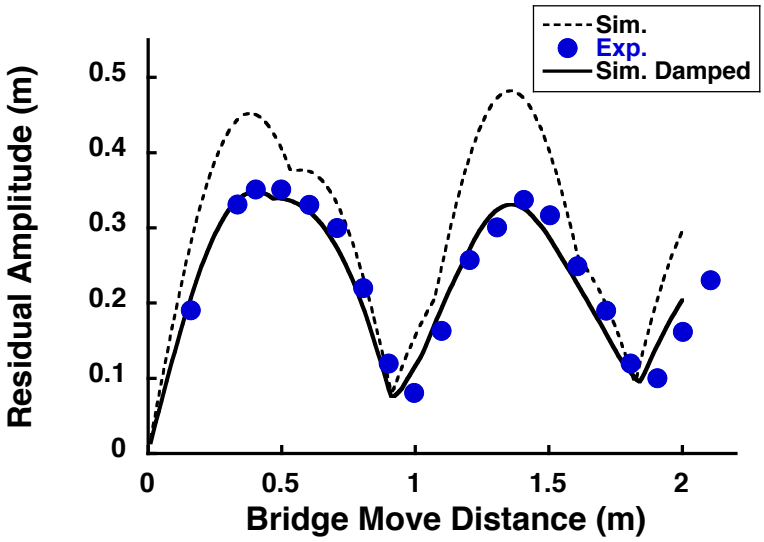

(a) Hook 1

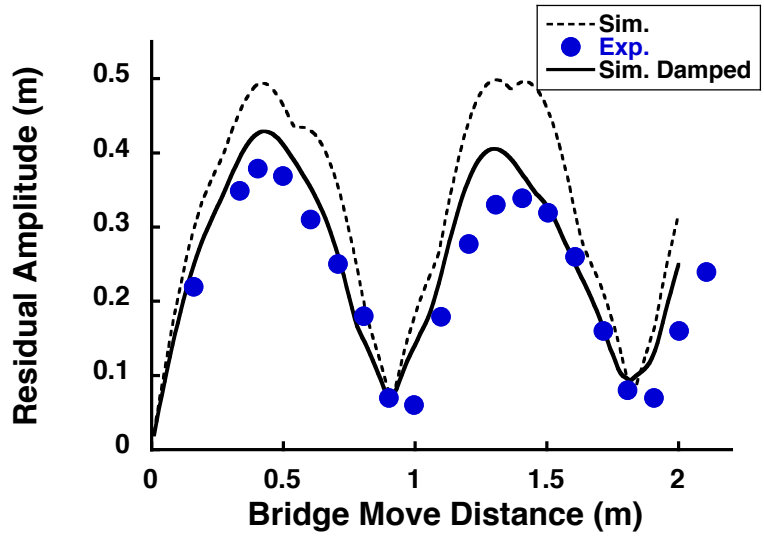

(b) Hook 2

Figure 4.9: Residual Amplitude Plot for a 70 kg Payload Mass

payload response for bridge motion compared to trolley motion because the surface area of the payload perpendicular to the direction of travel is much greater for bridge motions. The simulations were repeated with the damping parameters shown in Table 4.1. Figure 4.8 also shows the residual amplitude resulting from bridge movements with the modeled damping forces. Compared to the undamped model, the damped simulation curves have a much better resemblance to the experimental data.

For a heavier payload mass of 70 kg, Figure 4.9 shows the experimental, undamped simulation, and damped simulation peak-to-peak residual amplitude curves resulting from point-to-point bridge moves. The damped simulation curves, obtained using the same damping parameters from Table 4.1, are very similar to the experimental curves. The peaks from the experimental curves are still less than those from the undamped simulation. However, the undamped simulation and experimental curves have better agreement than those from the 7 kg payload. This is because the inertia of the system increases with a larger payload mass while the damping forces remain nearly unchanged. Therefore, the damping forces have a greater effect on the response of lighter payloads.

4.1.3 L-Shaped Bridge and Trolley Motions

This section investigates the dynamics for combined trolley and bridge motions. The parameters from Table 1.2 were used for the simulations. The crane first completed a trolley move, and then after a 0.5 s delay, executed a bridge move. After the bridge stopped moving, the residual peak-to-peak amplitude was calculated for both the bridge (x) and trolley (y) directions. Then, the total residual amplitude (RA) is:

$$RA_{total} = \sqrt{[RA_x]^2 + [RA_y]^2} \tag{4.1}$$

Each L-shaped motion was simulated for 60 s. For a 7 kg triangular payload, Figure 4.10 shows the total residual amplitude for L-shaped moves consisting of 0.4 m

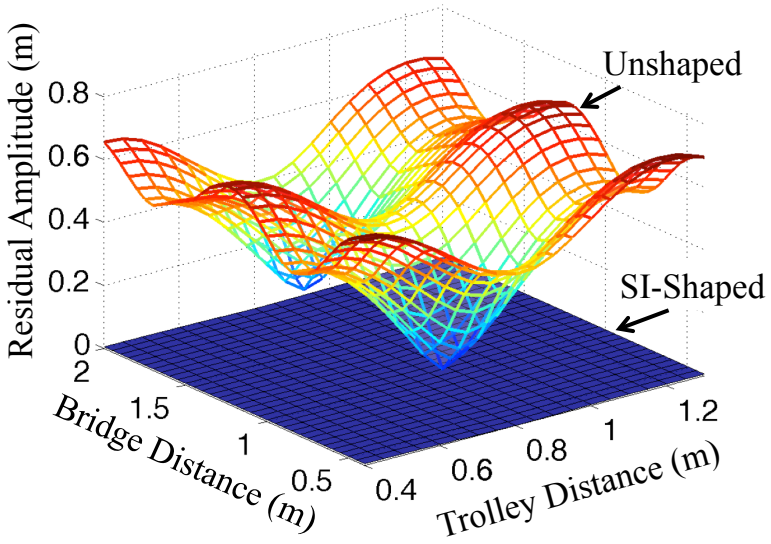

(a) Hook 1

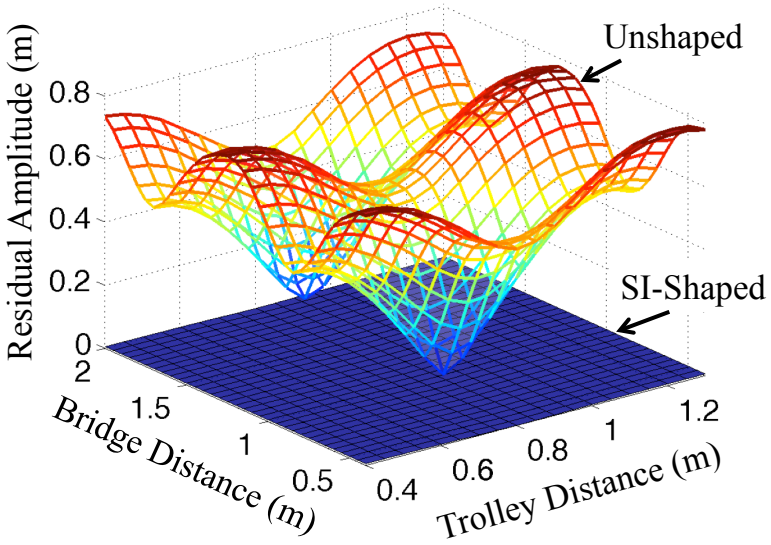

(b) Hook 2

Figure 4.10: Residual Amplitude for L-Shaped Moves (7 kg Payload Mass)

to 1.2 m trolley moves followed by 0.4 m to 2.0 m bridge moves. The mean ± standard deviation of the total residual amplitude for hook 1 and hook 2 is 0.49 m ± 0.13 m and 0.55 m ± 0.15 m, respectively. There are peaks and troughs corresponding with maximum and minimum levels of residual oscillation. However, most combinations of bridge and trolley moves result in considerable levels of residual oscillation.

Input shapers were designed to suppress the oscillation resulting from both bridge

and trolley motions. For trolley movements, a ZV shaper was designed to suppress the single 0.41 Hz mode:

$$\begin{bmatrix} A \\ t(ms) \end{bmatrix} = \begin{bmatrix} 0.5 & 0.5 \\ 0 & 1220 \end{bmatrix} \tag{4.2}$$

Bridge motion excites the swing (0.38 Hz), twist (0.45 Hz), and roll (0.79 Hz) modes. A three-mode SI shaper was designed with zero-vibration constraints at 0.38 Hz, 0.45 Hz, and 0.79 Hz:

$$\begin{bmatrix} A \\ t(ms) \end{bmatrix} = \begin{bmatrix} 0.178 & 0.120 & 0.202 & 0.211 & 0.112 & 0.177 \\ 0 & 934 & 994 & 1769 & 1855 & 2773 \end{bmatrix} \tag{4.3}$$

The L-shaped moves were repeated using the input shapers in (4.2) and (4.3) to shape the trolley and bridge movements, respectively. The residual amplitude resulting from these input-shaped movements are also shown in Figure 4.10. Input shaping reduced the residual amplitude to near-zero for every L-shaped move.

4.2 Analysis of Modal Coupling

This section uses simulations to investigate the level of coupling between the swing, twist, and roll modes that are induced by bridge motion. The frequency identification process from Section 3.3.1 was used to find the oscillation frequencies for each system configuration. Then, a process similar to the amplitude identification process from Section 3.3.2 was used to design input shapers to excite only a single mode. This input shaper was used to perform a bridge move, and the initial conditions required to excite only that single mode were determined from the time responses of ϕ_1, ϕ_2, θ_1, θ_2, β, γ, and ψ. Finally, these initial conditions were specified in the simulation model, and a new simulation was performed where the payload response was simulated for 300 s after the payload was released. The level of coupling between the modes

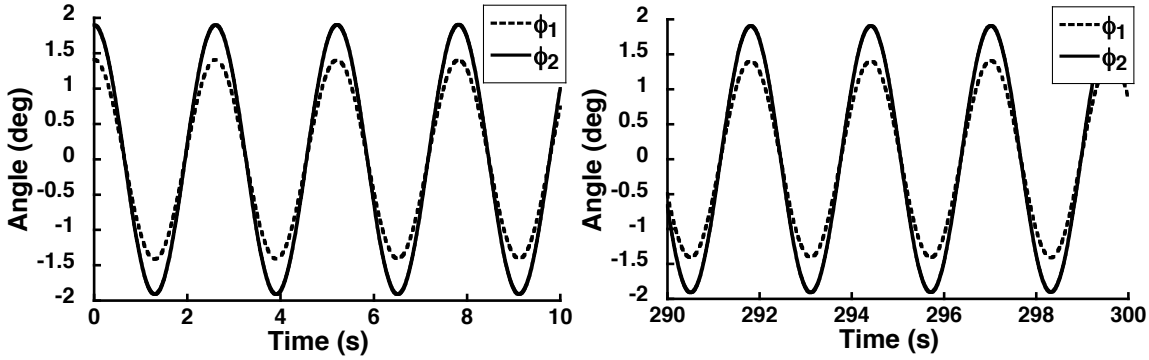

(a) Swing Mode – 0-10 s

(b) Swing Mode – 290-300 s

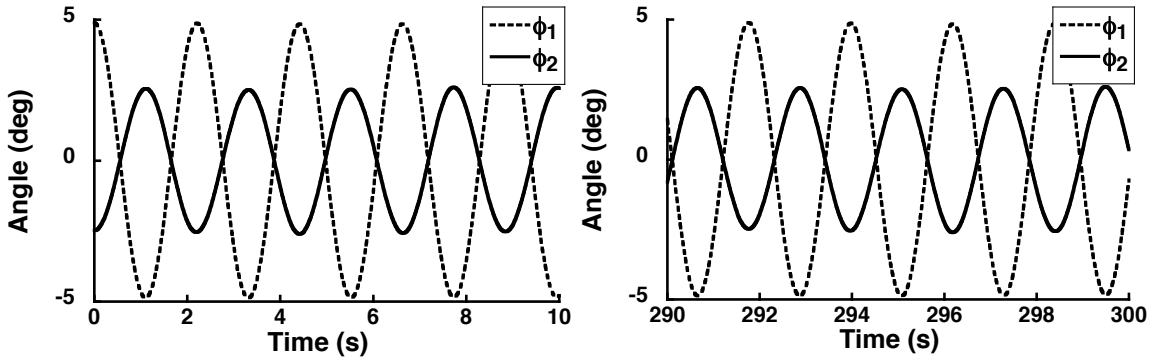

(c) Twist Mode – 0-10 s

(d) Twist Mode – 290-300 s

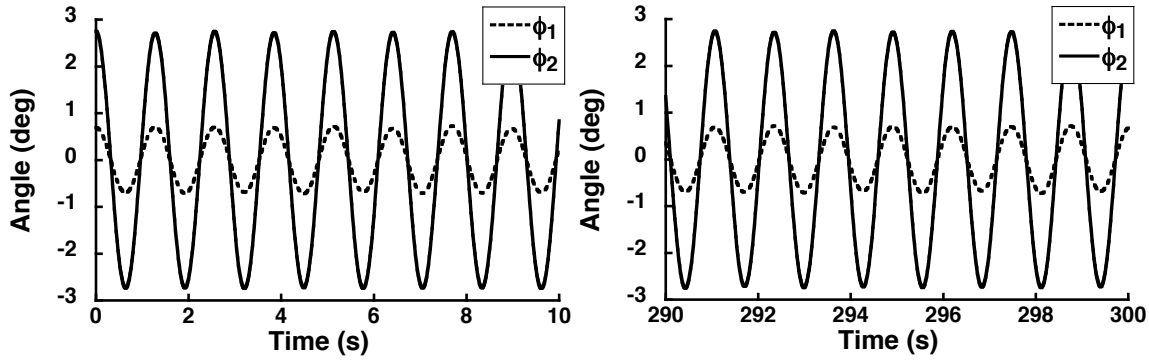

(e) Roll Mode – 0-10 s

(f) Roll Mode – 290-300 s

Figure 4.11: Modes Induced From Bridge Motion – Equal Cable Lengths

was investigated by plotting ϕ_1 and ϕ_2 and visually determining if there was energy exchange between the excited mode and the modes that were not initially excited.

The parameters listed in Table 1.2 were used for the first modal coupling analysis. The hook cable lengths, L_1 and L_2, were equal at 1.5 m. The trolley separation

distance and payload length were both 2.3 m. No damping was used. The initial conditions were specified to excite only one mode after the payload was released and allowed to oscillate. Figure 4.11 shows the hook responses for the swing, twist, and roll modes. The responses are shown from 0-10 s and 290-300 s in order to investigate if energy is transferred to the other modes over time. No modal coupling is evident from the time response plots of the swing, twist, and roll modes.

Next, modal coupling was investigated for unequal cable lengths. The parameters were the same as the previous analysis, except L_2 was changed to 1.0 m. The initial conditions were specified to excite only one mode after the payload was released and allowed to oscillate. Figure 4.12 shows the hook responses for the swing, twist, and roll modes. No modal coupling is evident.

4.3 Characterization of the Modes Induced by Bridge Motion

The Input-Shaped System Identification method described in Chapter 3 was used to determine how the dual-hoist crane system's modes change as a function of the triangular payload mass and geometry using simulations. As described in the frequency identification process from Section 3.3.1, input-shaped bridge moves were used to increase the signal-to-noise ratio of ϕ_1 and ϕ_2 for determining the modal frequencies. After the modal frequencies were characterized as a function of the system parameter, SMA-shaped bridge motions were used to determine the relative peak-to-peak hook-displacement amplitude of each mode that results from a single impulse. This amplitude identification process was described in Section 3.3.2. The reference command for the amplitude identification process was the first two impulses of the trapezoidal shaper. So, the residual vibration amplitudes were calculated while the crane was coasting with a velocity of $v_{max} = 0.33\ m/s$. The crane acceleration was a constant $a = 1\ m/s^2$. The nominal parameters used for the simulations were shown in Table 1.2.

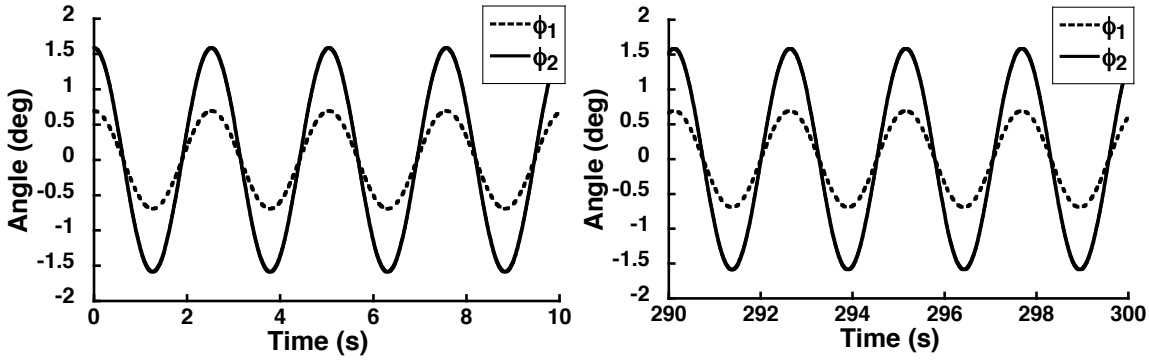

(a) Swing Mode – 0-10 s

(b) Swing Mode – 290-300 s

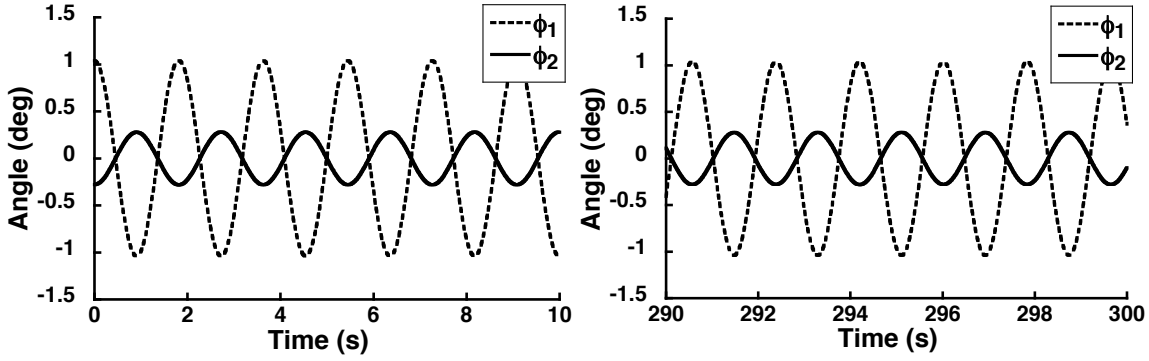

(c) Twist Mode – 0-10 s

(d) Twist Mode – 290-300 s

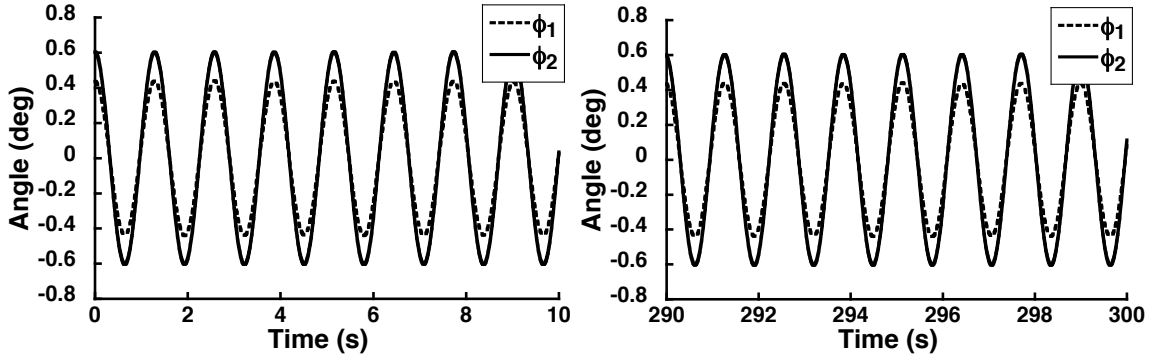

(e) Roll Mode – 0-10 s

(f) Roll Mode – 290-300 s

Figure 4.12: Modes Induced From Bridge Motion – Unequal Cable Lengths

4.3.1 Triangular Payload Mass

First, the modes were characterized for variations in the payload mass. In simulations, the crane was moved in the bridge direction with different triangular payload masses

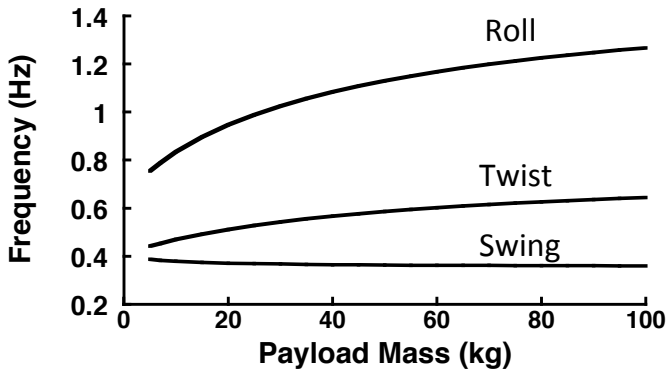

Figure 4.13: Oscillation Frequency vs. Payload Mass

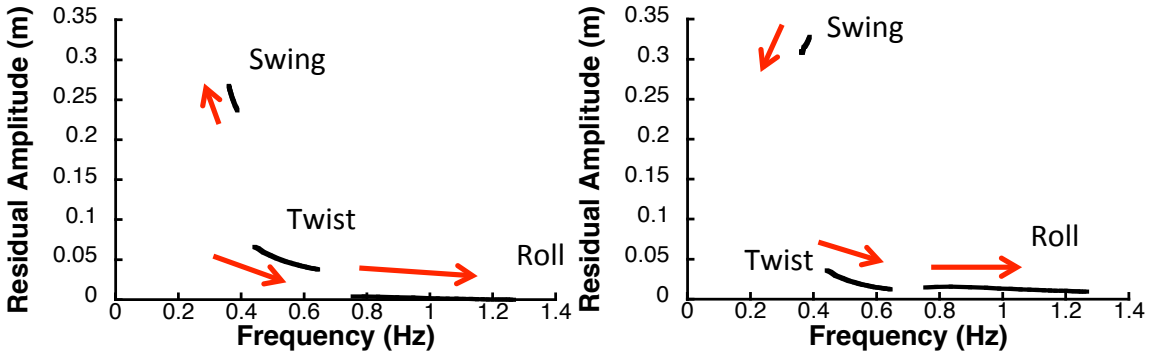

(a) Hook 1 (ϕ_1) **(b)** Hook 2 (ϕ_2)

Figure 4.14: Mode Residual Amplitude vs. Frequency (Payload Mass)

while the dimensions remained constant. Figure 4.13 shows the system's oscillation frequencies as a function of the payload mass. The lowest-frequency "swing" mode corresponds to the payload swinging like a pendulum from the trolley hoists. The middle-frequency "twist" mode corresponds to the twisting motion that was shown in Figure 1.5b. The highest-frequency "roll" mode corresponds to the rolling motion that was shown in Figure 1.5c.

Figure 4.14 shows the hook-displacement amplitude versus frequency of hook 1 and hook 2 for payload masses ranging from 5 kg to 100 kg. The red arrows indicate the direction of increasing payload mass. For both hooks, the pendulum swing mode is the largest component of the total response, and the frequency decreases as the payload mass is increased. The twist and roll mode frequencies increase with increasing mass.

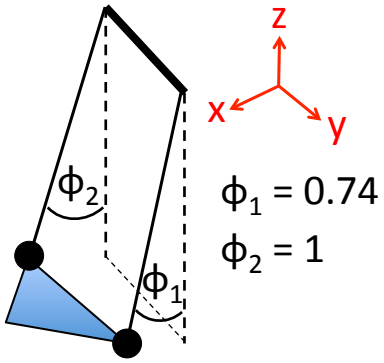

(a) Swing Mode Shape

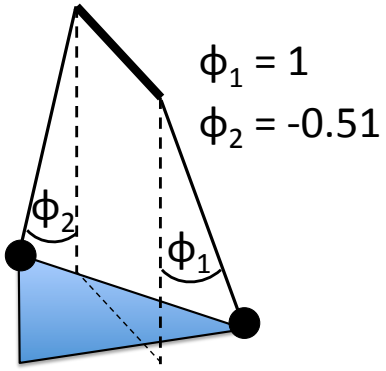

(b) Twist Mode Shape

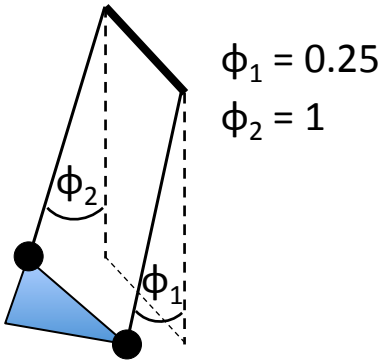

(c) Roll Mode Shape

Figure 4.15: Mode Shapes for 7 kg Payload

The mode amplitude decreases as the frequency increases for all but the swing mode of Hook 2.

In the amplitude identification process, SMA shapers are used to take energy out of all the modes except for one, which results in a one-mode response. Given such simplified responses, the mode shapes can be determined from two or more angles or

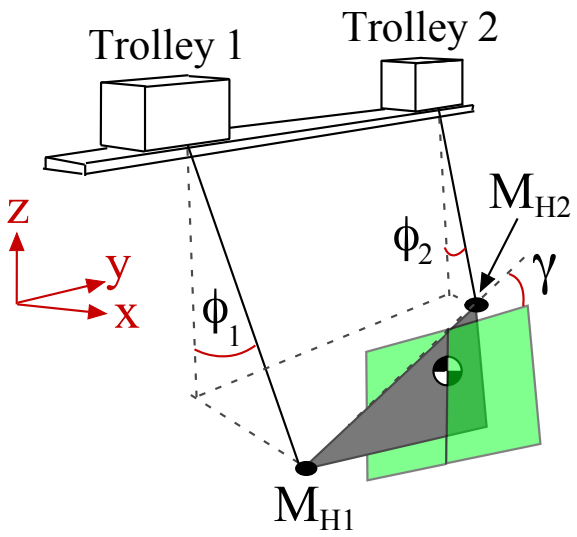

Figure 4.16: Twist Mode (γ)

points on the system. The ϕ_1 and ϕ_2 hook rotation angles were used to identify the mode shapes. The swing, twist, and roll mode shapes are shown in Figure 4.15 for a 7 kg payload.

Each mode affects ϕ_1 and ϕ_2 differently because of the geometry and rotational inertia of the triangular payload. Figure 4.16 illustrates why ϕ_1 has a larger amplitude than ϕ_2 for the twist mode. The green, vertical plane is parallel to the yz-plane and coincident with the payload's center of mass. When $\phi_1 = \phi_2 = 0$, then $\gamma = 0$. The pivot point for the twisting motion is the center of mass of the oscillating system, which consists of M_{H1}, M_{H2}, and the payload mass. Hook 1 is further away from the center of mass than hook 2, so hook 1 moves a greater distance for the same rotation angle.

For the roll mode, ϕ_2 has a larger residual amplitude than ϕ_1. This can be explained in terms of the mass distribution of the payload between the two hooks. During the rolling motion, the payload's center of mass moves in the x-direction, as indicated in Figure 4.16. The hooks move in the opposite direction to compensate. However, a greater percentage of the payload mass is concentrated under hook 2, so

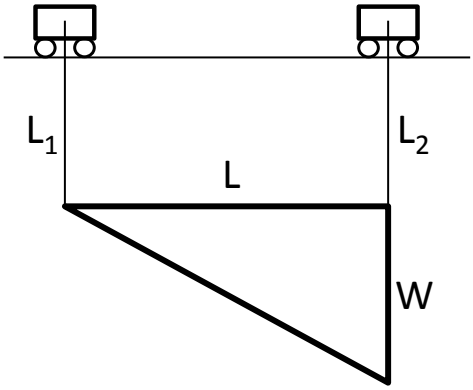

Figure 4.17: Sketch of the Triangular Payload Configuration

hook 2 has to move a greater distance.

4.3.2 Triangular Payload Width

To study the effect of the payload width (W), it was incremented from 0.1 m to 4 m, while maintaining a constant payload mass. A sketch of the triangular payload configuration is shown in Figure 4.17. Figure 4.18 shows the effect of the payload width on the three mode frequencies for constant payload masses of 7 kg and 70 kg. As the width increases, both the swing and roll frequencies decrease because the payload's center of mass moves closer to the ground, which increases the effective pendulum length for both modes. The twist frequency remains approximately constant when the width is changed, but increases as the payload mass becomes greater.

Figure 4.19 shows the hook-displacement amplitude versus frequency of hook 1 and hook 2 when the payload width is incremented from 0.1 m to 4.0 m for payload masses of 7 kg and 70 kg. The red arrows indicate the direction of increasing payload width. For hook 1, the swing and twist modes contribute significantly to the overall amplitude. As the width is increased, the swing amplitude decreases while the twist amplitude increases. In fact, the twist mode becomes more significant than the swing mode for the 7 kg payload mass as the width is increased. For hook 2, swing and roll are significant to the total response. With increasing width, the swing amplitude

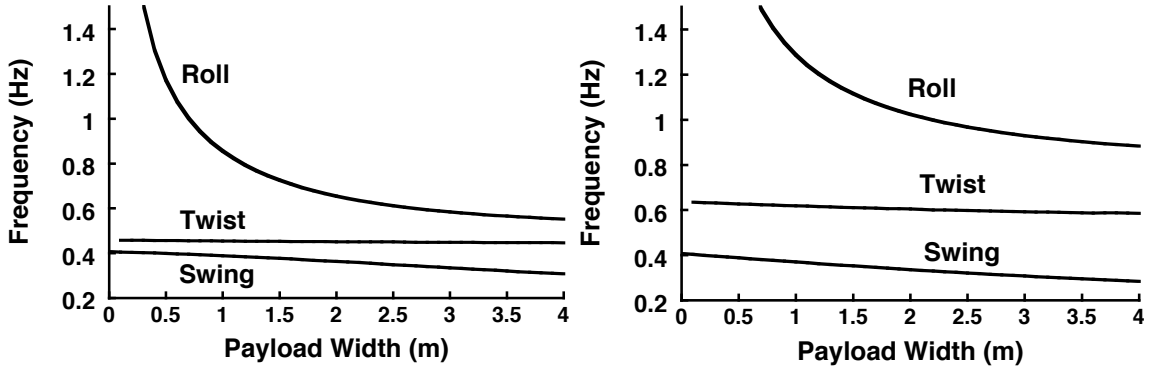

(a) 7 kg Payload Mass **(b)** 70 kg Payload Mass

Figure 4.18: Oscillation Frequency vs. Payload Width

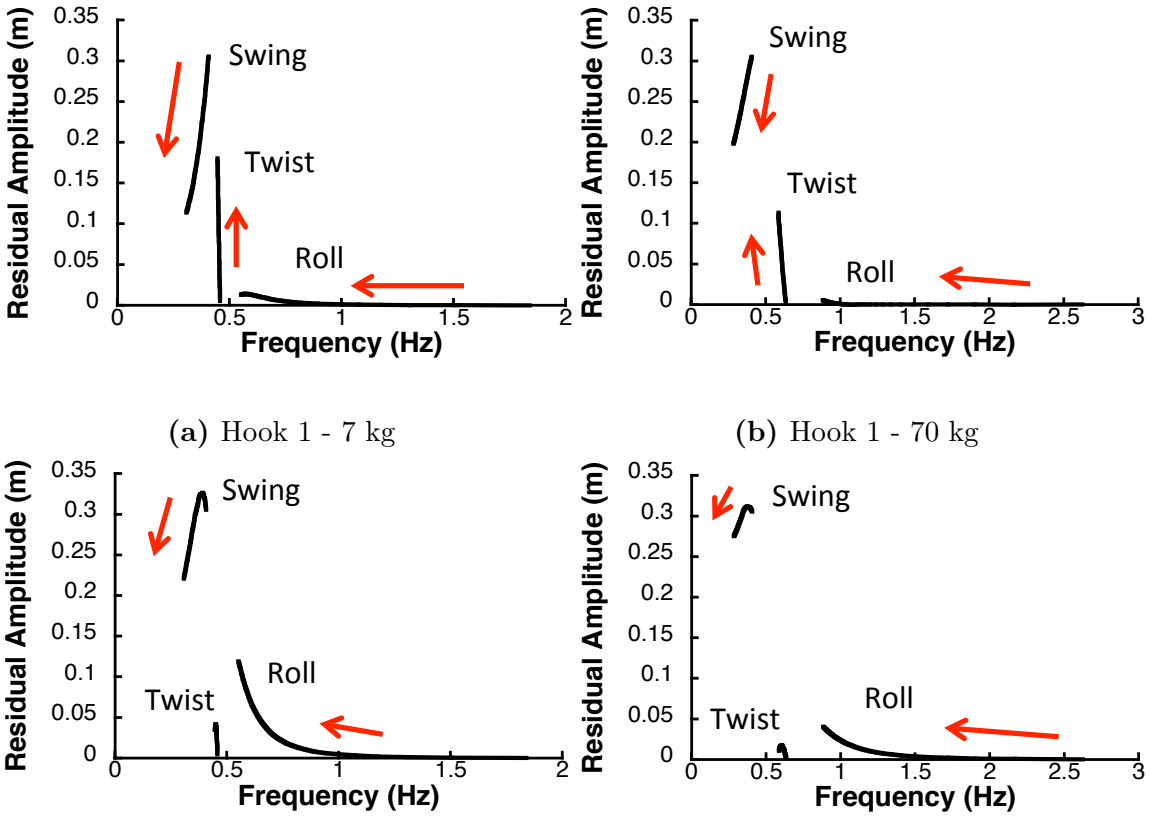

(a) Hook 1 - 7 kg **(b)** Hook 1 - 70 kg

(c) Hook 2 - 7 kg **(d)** Hook 2 - 70 kg

Figure 4.19: Mode Residual Amplitude vs. Frequency (Payload Width)

decreases and the roll amplitude increases. For both hooks, the mode amplitudes shift more for the lighter payload.

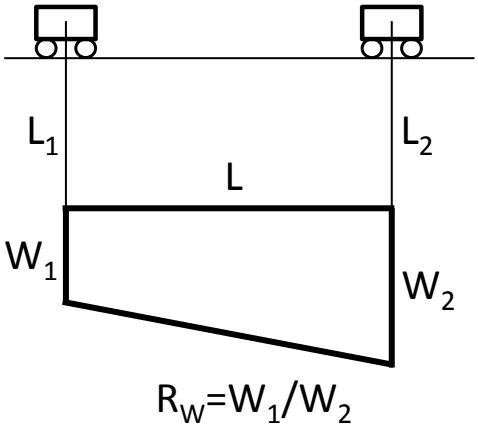

Figure 4.20: Right-Trapezoidal Payload

4.3.3 Right-Trapezoidal Payload Width Ratio

Next, the dynamics were investigated for the right-trapezoidal payload configuration shown in Figure 4.20. The right-trapezoidal payload is created by adding a second width dimension, W_1, below hook 1. The width dimension beneath hook 2 is W_2. With a constant $W_2 = 1.2$ m, the mode frequencies and maximum residual amplitudes were investigated with W_1 ranging from 0 m to 4 m. The payload width ratio, R_W, is:

$$R_W = W_1/W_2 \tag{4.4}$$

All other parameters are specified in Table 1.2. The mode frequencies versus R_W are shown in Figure 4.21 for payload masses of 7 kg and 70 kg. The swing and roll frequencies decrease as R_W increases because the effective pendulum length of both modes increases. As the payload mass increases, the twist and roll frequencies shift upwards while the swing frequency shifts slightly downwards.

Figure 4.22 shows the hook-displacement amplitude versus frequency of hook 1 and hook 2 when the payload width ratio is incremented from 0 to 3.3 for payload masses of 7 kg and 70 kg. The red arrows indicate the direction of increasing width ratio.

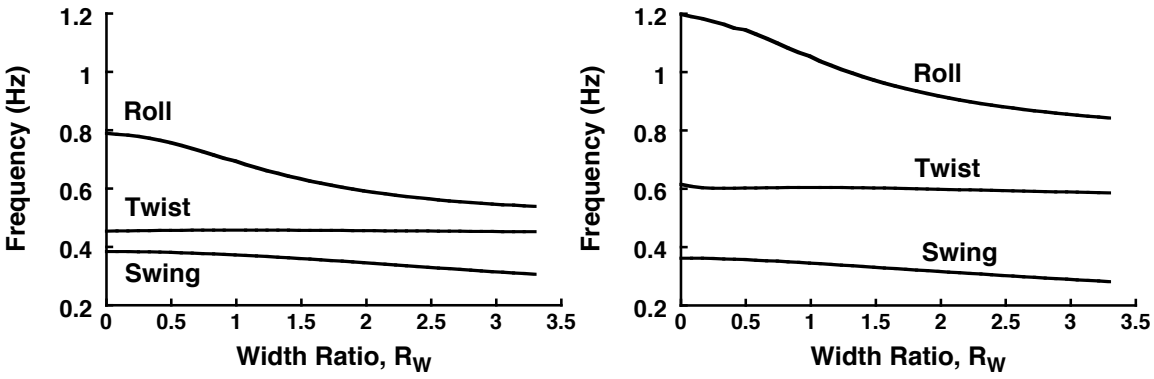

(a) 7 kg Payload Mass **(b)** 70 kg Payload Mass

Figure 4.21: Oscillation Frequency vs. R_W for Bridge Motion

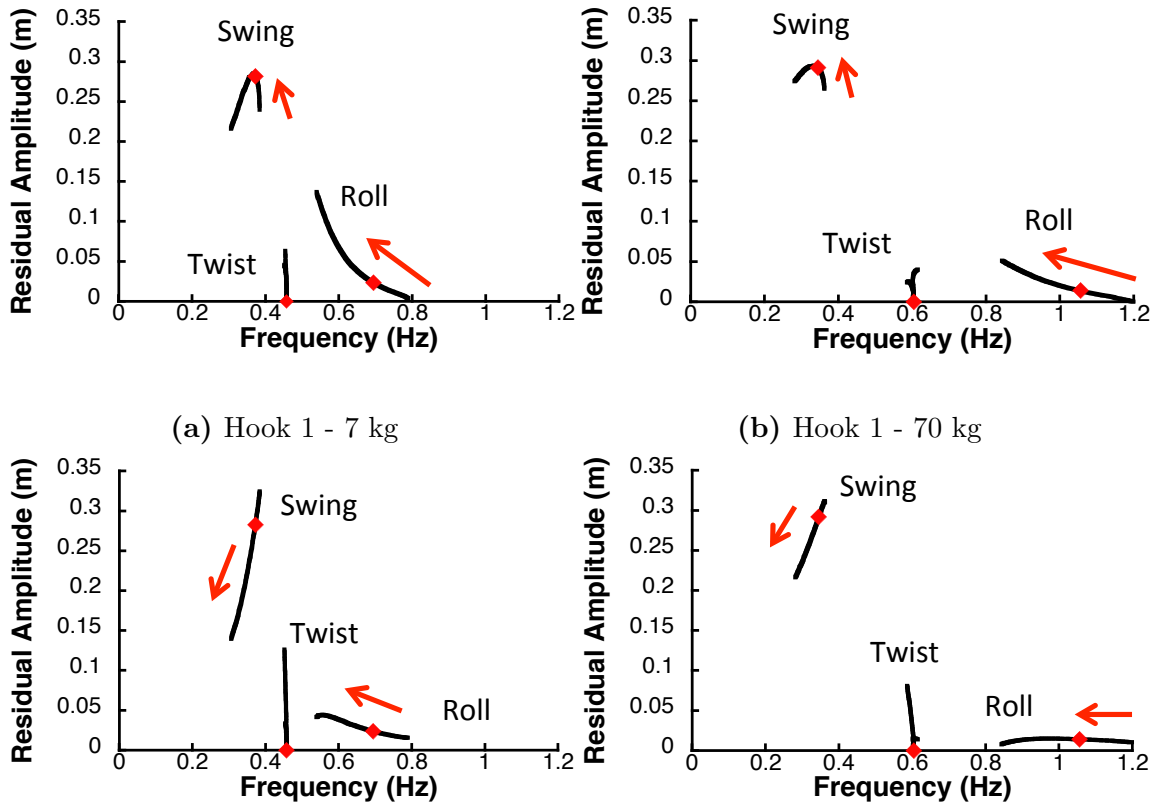

(a) Hook 1 - 7 kg **(b)** Hook 1 - 70 kg

(c) Hook 2 - 7 kg **(d)** Hook 2 - 70 kg

Figure 4.22: Mode Residual Amplitude vs. Frequency (R_W)

The red points are plotted when $R_W = 1$, which represents a rectangular payload when W_1 and W_2 are equal. The twist amplitude is zero for both hooks when R_W is unity because the center of mass is equidistant between the two hooks and no moment is induced during bridge motions. However, the twist mode could be excited if an external force is applied to the payload, such as in a collision. The amplitude increases as R_W moves in either direction away from unity. The swing amplitude for hook 1 first increases with R_W, then has a maximum value when $R_W = 1$, and finally decreases as $R_W > 1$. Also, the roll amplitude for hook 1 increases with R_W as the center of mass moves closer to hook 1. For hook 2, the swing amplitude decreases as R_W increases, and the roll amplitude is the least significant contributor to the total response except when R_W is close to unity.

This chapter investigated the dynamic response of a dual-hoist bridge crane moving distributed payloads using simulations and experiments. Trolley motion caused the payload to oscillate with a single frequency, and a ZV shaper was effective for reducing this type of payload oscillation. Bridge motion induced a three-mode response. The three modes were characterized for variations in the payload mass and geometry. An input shaper designed for all three modes, such as a three-mode SI shaper, was shown to be effective at reducing payload oscillation induced by bridge motions. Finally, separate input shapers designed for trolley and bridge motions were shown to be effective at reducing payload oscillation induced by L-shaped trolley and bridge motions. Insights from the dynamic analysis were used to design input shapers for Chapter 5, where human operator studies were completed to determine the effect input shaping has on human operator performance when driving a triangular payload through an obstacle course with a dual-hoist bridge crane.

CHAPTER V

OPERATOR STUDIES

Operator studies were conducted to investigate how people control dual-hoist cranes carrying distributed payloads. Insights from the dynamic analysis in Chapter 4 were used to design input shapers for a given crane configuration to reduce payload oscillation caused by bridge and trolley motions. Trials were completed both with and without input shaping to determine the effect input shaping has on task completion time and operator effort.

5.1 Operator Test Protocol

5.1.1 Physical Setup

Figure 5.1 is an annotated photograph of the crane with the cable lengths and payload dimensions used for the operator studies. The cable lengths were set to 1.5 m. The payload has a length of 2.4 m and a width of 1.2 m. The trolley separation distance was 2.4 m.

Figure 5.2 is an overhead sketch that illustrates the obstacle course setup and the nominal path for completing the task. The required task is to move the payload from the starting point to the target area as fast as possible without colliding with the obstacles. Operators were not allowed to change the suspension cable lengths, so operators needed to transport the payload between the two obstacles. The separation distance between the two obstacles is SD_{obs}.

Figure 5.3 and Figure 5.4 show that each end of the payload was equipped with laser pointers. The lasers place markers on the ground to clearly show the position of the payload with respect to the ground.

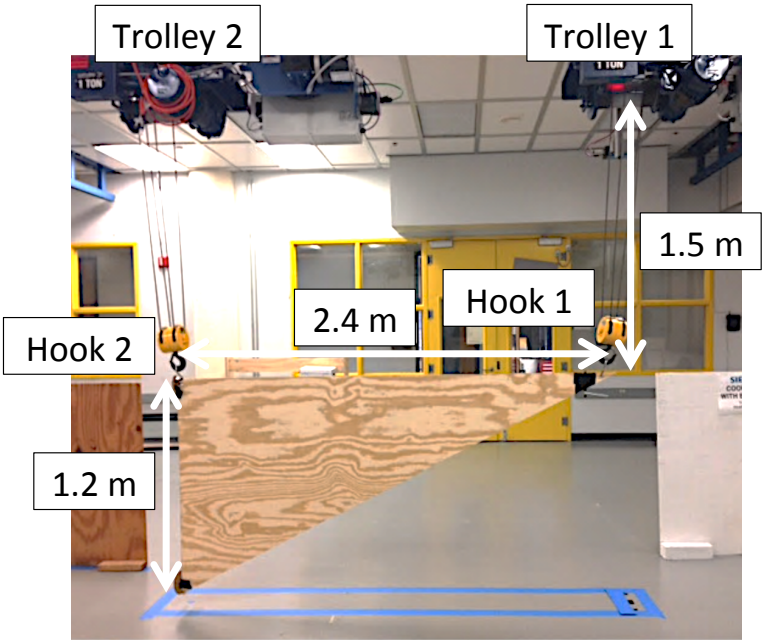

Figure 5.1: Dual-Hoist Bridge Crane Test Configuration

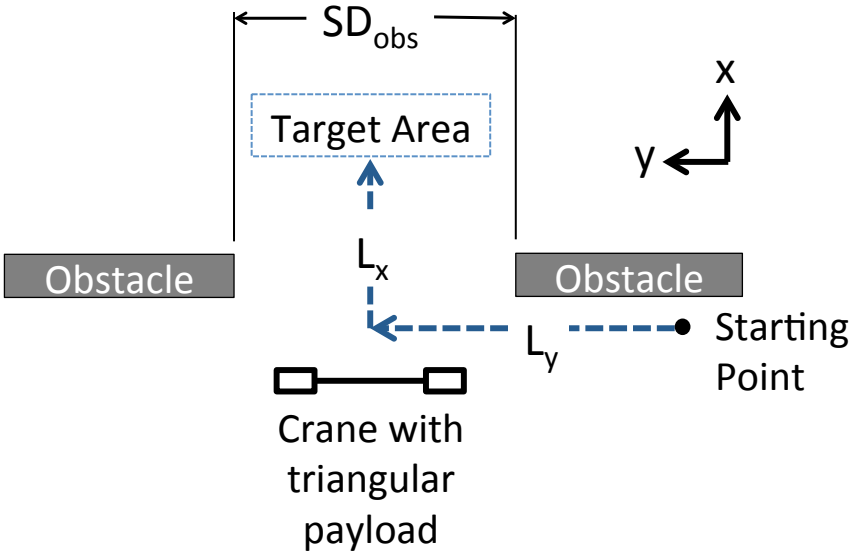

Figure 5.2: Obstacle Course Setup

5.1.2 Procedure

Each test subject practiced driving the crane for approximately two minutes with input shaping and two minutes without input shaping to become familiarized with the control of the crane prior to the actual experiment. Figure 5.3 shows the view of

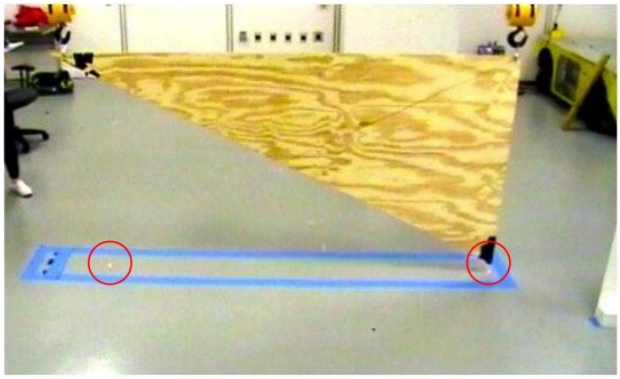

Figure 5.3: Camera Field of View

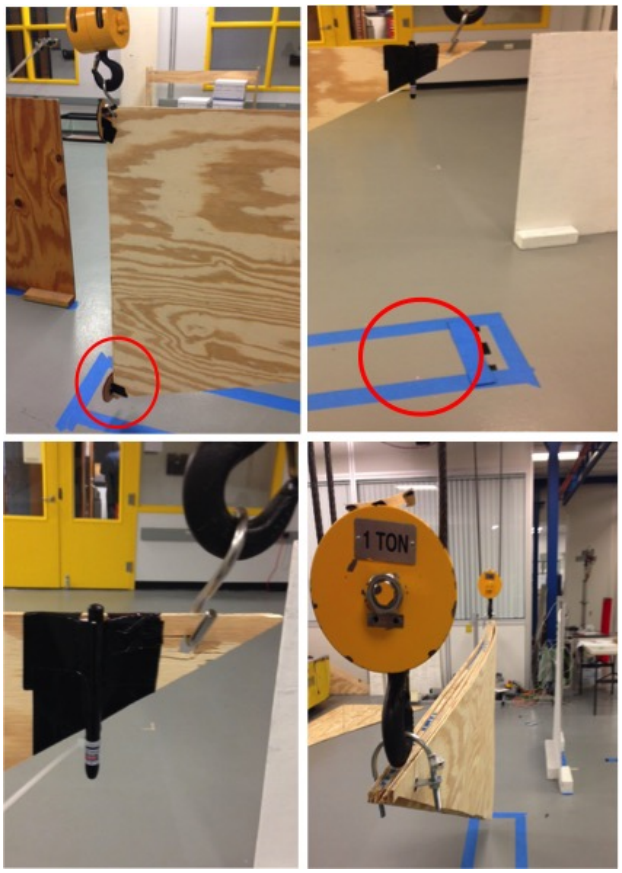

Figure 5.4: Dual-Hoist Bridge Crane Components

the video camera for recording each test. The course completion time was measured from initial crane motion to when the two laser markers entered and remained within the rectangular target boundary on the ground by using a stopwatch to manually measure the time. Each test run was recorded on video so that each test could be

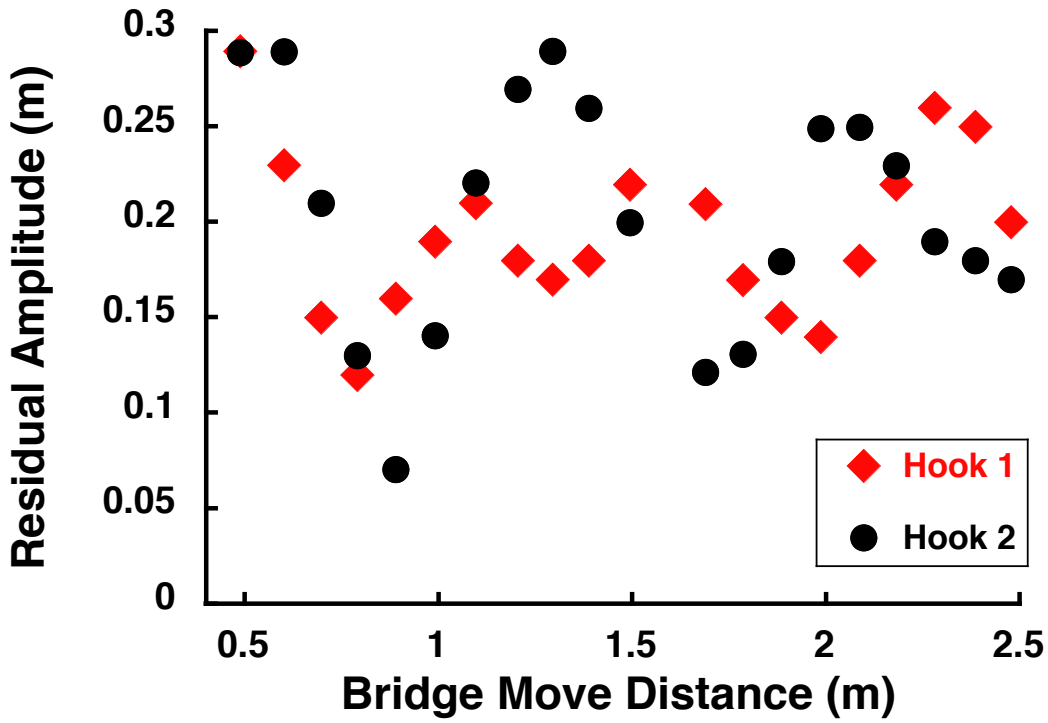

Figure 5.5: Residual Amplitude Plot for Bridge Motions

verified to ensure accuracy.

Three different operator studies were completed. The first study used bridge and trolley move distances that resulted in large residual amplitudes from point-to-point moves. The second study increased the range of bridge move distances to include both large and small residual amplitudes resulting from point-to-point moves. The third study used three different triangular payload masses and had bridge and trolley move distances that corresponded to maximum, intermediate, and minimum levels of residual oscillation resulting from point-to-point moves.

In each study, bridge and trolley move distances were chosen based on the amount of residual oscillation that ensues from point-to-point moves. Figure 5.5 shows the experimentally determined residual oscillation curve for point-to-point bridge moves. The residual amplitudes are the peak-to-peak displacement amplitudes of hook 1 and hook 2. This curve was determined using the crane configuration used for the operator studies that was shown in Figure 5.1, with a 7 kg triangular payload.

Crane applications usually require altering the cable lengths during operation. A ZV shaper is not very robust to variation in frequency (i.e. cable length changes). Therefore, a more robust shaper, such as an Extra-Insensitive (EI) shaper [20] or a Specified-Insensitivity (SI) shaper [21], should be implemented in applications with significant hoisting to provide adequate robustness.

5.2 Maximum Bridge Oscillation Study

The first study, called the Maximum Bridge Oscillation (MBO) study, used bridge move distances that resulted in maximum levels of residual oscillation from point-to-point moves. So, if the operator issued a command (by pressing a directional button on the HMI) that moved the bridge a distance that was within the selected move distance range, then the hook oscillation amplitudes would be near the peak of the residual oscillation curve, such as those shown in Figure 5.5. However, if the operator used multiple button pushes to move the crane the same distance, then the oscillation amplitude could be greater or smaller than the peak oscillation curve amount.

The bridge direction (L_x) move distance range varied between 1.1 m to 1.4 m in 0.1 m increments. This move distance range was chosen because it resulted in large residual oscillation amplitudes for both hook 1 and hook 2, as shown in Figure 5.5. The trolley move distance was selected to result in large residual oscillation from a point-to-point move and was held constant. As shown in Figure 5.2, obstacles were placed in the course to increase the difficulty of the task. The two obstacles were spaced 3.5 m apart.

Starting from an L_x of 1.1 m, each of the seven test subjects completed a test run using unshaped control and then using input-shaped control. This was repeated for bridge move distances of 1.2 m, 1.3 m, and 1.4 m, for a total of 8 test runs per operator.

The payload response was different for trolley and bridge motions because of the

inertia properties of the payload. Therefore, one input shaper was utilized for trolley motion, and another input shaper was utilized for bridge motion.

A Zero Vibration (ZV) input shaper [8] was used for trolley 1 and trolley 2 motion along the bridge. The ZV input shaper, designed to cancel 0.43 Hz ($\zeta = 0$), has impulse values of:

$$\begin{bmatrix} t(ms) \\ A \end{bmatrix} = \begin{bmatrix} 0 & 1163 \\ 0.5 & 0.5 \end{bmatrix} \tag{5.1}$$

For bridge motion, a two-mode convolved ZV shaper [18] was used to cancel 0.39 Hz ($\zeta = 0$) and 0.755 Hz ($\zeta = 0$). These two frequency values were determined from experimental data. This shaper is:

$$\begin{bmatrix} t(ms) \\ A \end{bmatrix} = \begin{bmatrix} 0 & 662 & 1282 & 1944 \\ 0.25 & 0.25 & 0.25 & 0.25 \end{bmatrix} \tag{5.2}$$

The following data were collected for each test run:

- Test number
- Bridge move distance
- Controller setting (e.g., shaped or unshaped)
- Course completion Time, t_c
- Number of obstacle collisions

5.2.1 Maximum Bridge Oscillation Study Results

For the MBO study, the task completion times of operators 1-7 for each L_x distance are plotted in Figure 5.6. Faster completion times resulted when input shaping was used with the exception of subject 5 at $L_x = 1.1$ m and 1.4 m. This could be because subject 5 used a control technique that was different from the other operators, where rapid button pushes were used to move the crane. On average, the operators completed the course 47% faster with the aid of input shaping.

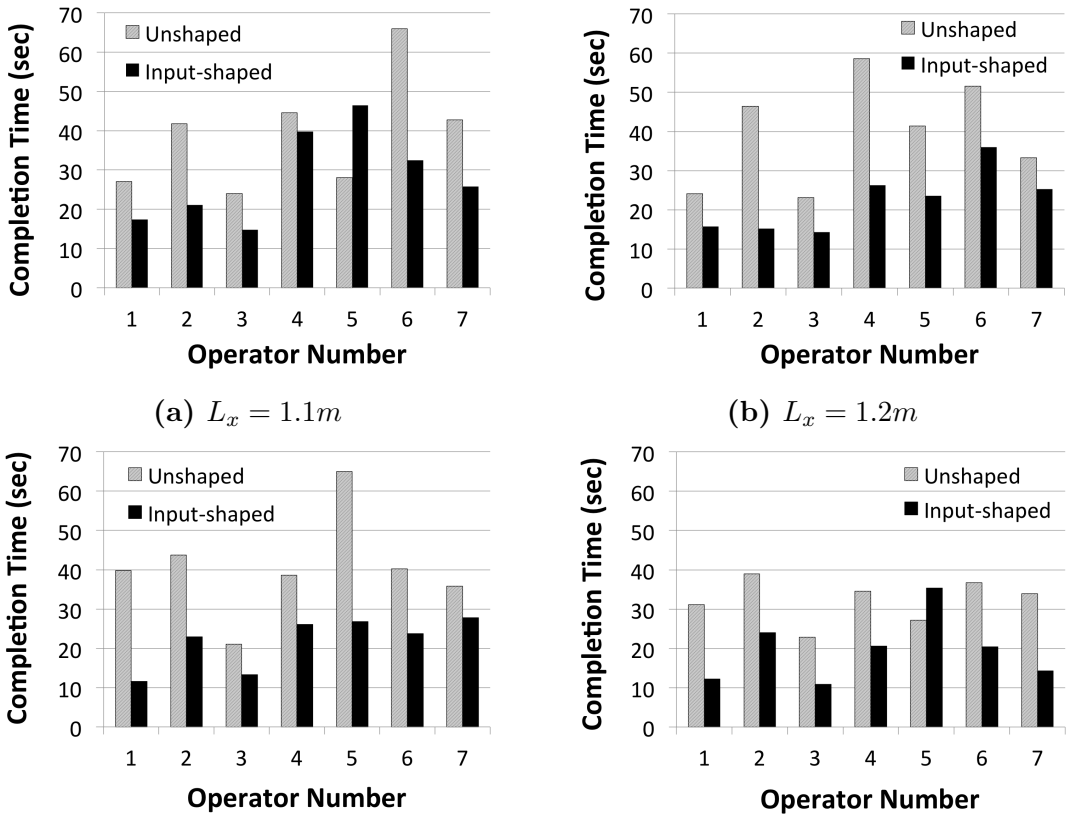

(a) $L_x = 1.1m$ **(b)** $L_x = 1.2m$

(c) $L_x = 1.3m$ **(d)** $L_x = 1.4m$

Figure 5.6: Operator Completion Times for MBO Study

Figure 5.7 shows a box plot of the shaped and unshaped completion times. A one-way ANOVA was performed to determine if differences between the means were statistically significant. Input shaping had a significant effect on completion time at the $p < 0.001$ level for the two conditions tested $[F(1, 54) = 27.73, p = 2.48 \times 10^{-6}]$.

The average completion time was calculated for all runs that used input shaping and for all runs that used standard control, respectively. Then, the completion time residuals for the shaped test condition were determined by subtracting the average shaped completion time from each individual shaped completion time. This was also done for the unshaped data. The results are plotted in Figure 5.8. If the data points fall on a line, then the data represents a normal distribution. From the graph, it is apparent that the data resembles a normal distribution except at the extremes.

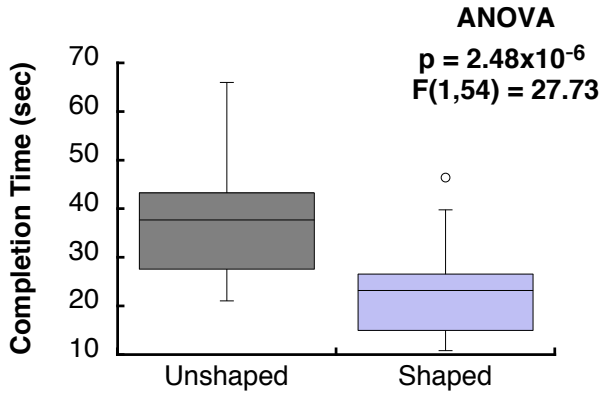

Figure 5.7: Box Plot of MBO Study Completion Times

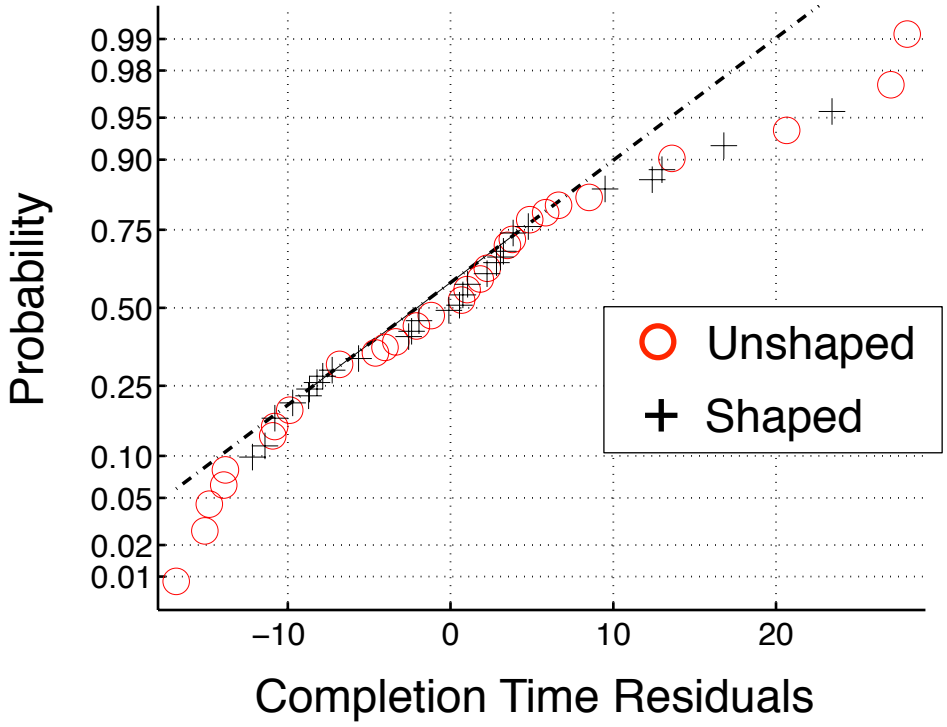

Figure 5.8: MBO Study Completion Time Residuals

5.3 Complete Bridge Oscillation Study

The second study, called the Complete Bridge Ocillation (CBO) study, increased the range of bridge move distances to include both high and low levels of residual oscillation resulting from point-to-point moves. The same trolley move distance from the MBO study was used. The trolley move distance was selected to result in large

residual oscillation from a point-to-point move and was held constant.

The bridge move distance range was increased to 1-2 m with 0.1 m increments. This range was chosen because it resulted in both maximum and minimum levels of residual oscillation, which is evident from the residual oscillation curve in Figure 5.5. It was not feasible to have each operator complete tests at each value of L_x, so each operator completed only four randomly determined bridge move distances both with and without input shaping, for a total of eight tests per operator. The order of the eight tests was randomized.

The ZV shaper in (5.1) from the MBO study was used for trolley motion. A two-mode Specified Insensitivity (SI) shaper [20, 10] was utilized for bridge motion. The two-mode SI shaper was designed to suppress frequency ranges of 0.39 Hz ($\zeta = 0.065$) and 0.75-0.76 Hz ($\zeta = 0.03$) to 5% of the unshaped level. The damping ratios were determined experimentally using the Logarithmic Decrement method. The shaper is:

$$\begin{bmatrix} t(ms) \\ A \end{bmatrix} = \begin{bmatrix} 0 & 845 & 1695 \\ 0.361 & 0.361 & 0.278 \end{bmatrix} \tag{5.3}$$

The operator moves the crane by pressing directional buttons on the HMI. The operator effort can be quantified by measuring the number of interface button pushes used to complete the obstacle course. The state of each button changes from zero (OFF) to one (ON) when the button is pressed. The directional button states were recorded by the PLC for each test run. From this data, the number of button pushes was determined to provide a quantifiable measure of the operator effort.

The following data were collected for each test run:

- Test number
- Bridge move distance
- Controller setting (e.g., shaped or unshaped)
- Course completion Time, t_c
- Number of obstacle collisions

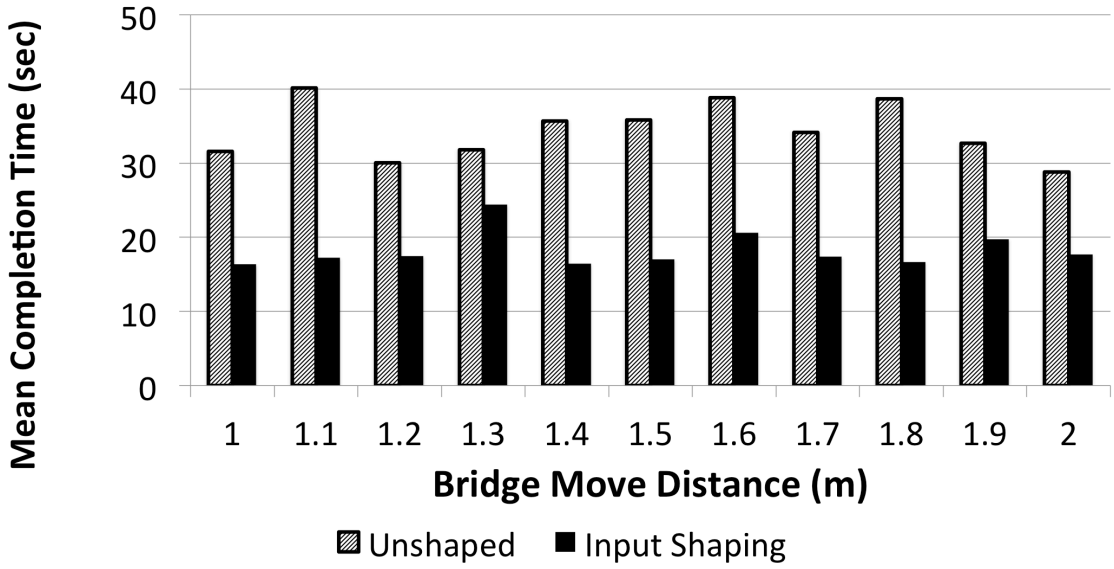

Figure 5.9: Average Completion Time for Each Bridge Move Distance

- Number of button pushes

5.3.1 Complete Bridge Oscillation Study Results

The results of the CBO study for the 15 test subjects are represented in Figure 5.9, where average course completion time is shown for each bridge move distance. The overall average completion time for the unshaped control mode is 35 seconds compared to only 18 seconds with input shaping. This amounts to an average time savings of 51% with input shaping.

The average number of button pushes are shown for each bridge move distance in Figure 5.10. Less button pushes were required on average to complete the course with the aid of input shaping, indicating that input-shaping control required less operator effort.

Figure 5.11 shows a box plot of the shaped and unshaped completion times from the CBO phase. A one-way ANOVA was performed to determine if differences between the means were statistically significant. Input shaping had a significant effect on completion time at the $p < 0.001$ level for the two conditions tested $[F(1, 118) = 173, p = 6.49 \times 10^{-25}]$.

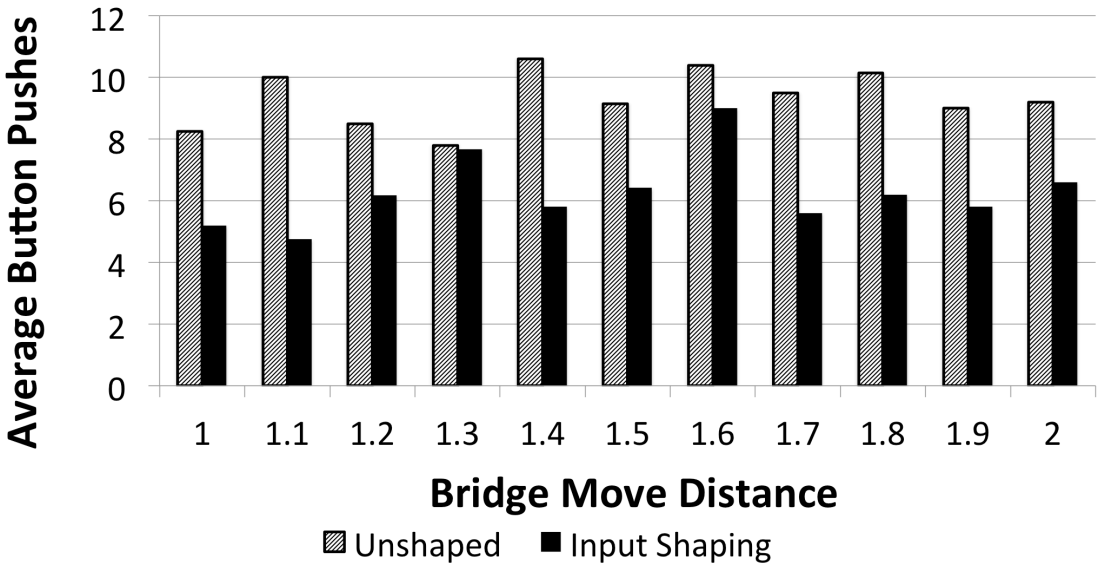

Figure 5.10: Average Number of Button Pushes

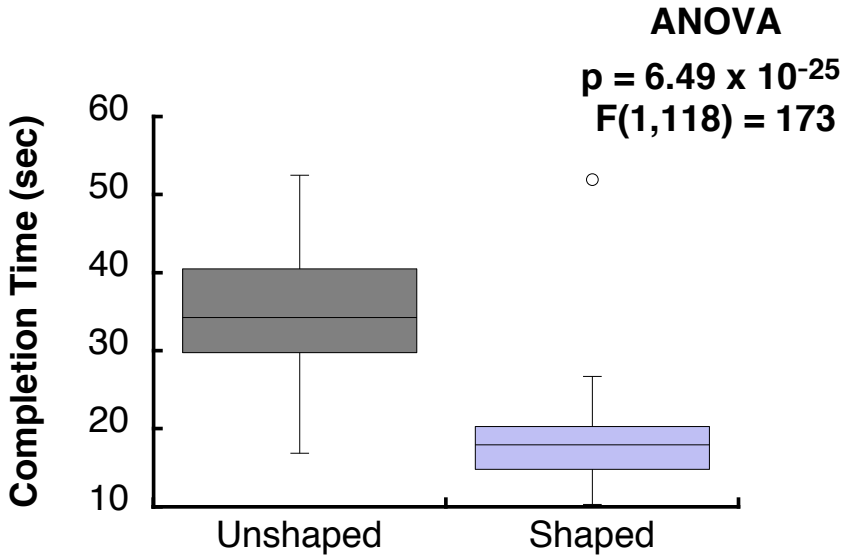

Figure 5.11: Box Plot of CBO Study Completion Times

The completion time residuals were calculated for the input-shaped and unshaped data. The results are plotted in Figure 5.12. If the data points fall on a line, then the data represents a normal distribution. From the graph, it is apparent that the data closely represents a normal distribution except for one outlier from the shaped group.

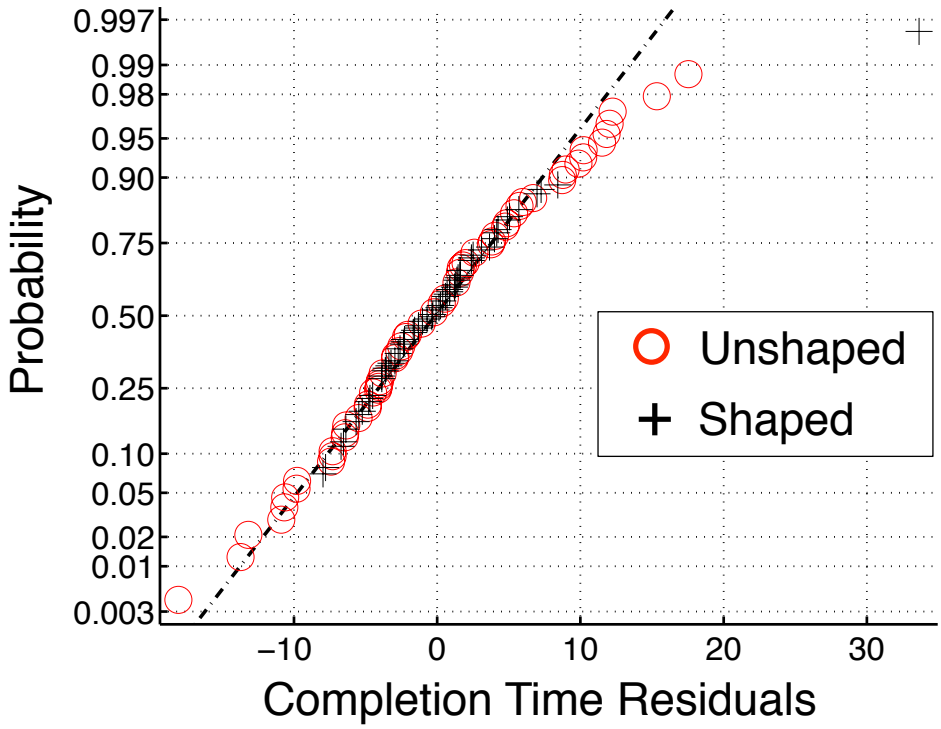

Figure 5.12: CBO Study Completion Time Residuals

5.4 Payload Mass, Bridge, and Trolley Study

The analysis from Chapter 4 revealed that the payload dynamics change as the payload mass is increased, so the Payload Mass, Bridge, and Trolley (PMBT) study varied the payload masses in order to investigate its effects. Three move distances were selected for both the bridge and trolley axes which resulted in maximum, intermediate, and minimum residual amplitudes from point-to-point moves, respectively. Table 5.1 shows the PMBT study parameters.

Three payload masses were used: 7 kg, 35 kg, and 63 kg. The 7 kg payload was a single piece of triangular plywood, as was shown in Figure 5.1. The 35 kg and 63 kg payloads were created by attaching five and nine triangular plywood pieces, respectively, to the hooks. Twelve subjects participated in the PMBT study. The PMBT study plan in Figure 5.13 lists the bridge and trolley move distances and the payload mass for each participant. Each subject was assigned two bridge and two

Table 5.1: PMBT Study Parameters

Parameter	**Value**
Payload Mass, M	7 kg, 35 kg, 63 kg
Payload Length , L	2.4 m
Payload Base, B	1.2 m
Cable Lengths, L_1 and L_2	1.5 m
Trolley Separation Distance, $SD_{trolley}$	2.4 m
Trolley Move Distances, $L_{y,max}$, $L_{y,med}$, $L_{y,min}$	1.15 m, 0.95 m, 0.80 m
Bridge Move Distances, $L_{x,max}$, $L_{x,med}$, $L_{x,min}$	1.35 m, 1.10 m, 0.90 m
Obstacle Separation Distance, SD_{obs}	2.9 m

Payload Mass (kg)	Test Subject	Bridge Move Distance (m)			Trolley Move Distance (m)		
		1.35	1.10	0.90	1.15	0.95	0.80
7	1	*		*	*	*	
	2		*	*		*	*
	3	*	*		*		*
35	4	*	*		*	*	
	5		*	*	*		*
	6	*		*		*	*
	7		*	*		*	*
63	8	*	*		*		*
	9		*	*		*	*
7 & 63	10	*		*	*		*
	11	*	*		*	*	
	12		*	*		*	*

Figure 5.13: PMBT Study Plan

trolley move distances, and completed all move combinations with and without input shaping for a total of eight test runs per subject. The test run order was randomized. Test subjects 10-12 completed the study twice using the 7 kg and 63 kg payloads to test for an interaction effect between the payload mass and controller type.

Table 5.2: Three-Mode SI Shaper Parameters for Bridge Motion in PMBT Study

Mode	**Frequency (Hz)**	**Damping Ratio**	**Vibration Limit (%)**
Swing	0.36 - 0.38	0.03	5
Twist	0.45 - 0.62	0.03	15
Roll	0.75 - 1.20	0.02	15

Because there were no obstacle collisions in the previous two studies, the obstacle separation distance was decreased from 3.5 m to 2.4 m in order to increase the task difficulty. A separation distance of 2.9 m was chosen because it is the sum of the payload length (2.4 m) and the maximum residual oscillation amplitude (0.5 m) induced by point-to-point trolley moves.

For trolley motion, the same ZV shaper in (5.1) was used to suppress the 0.43 Hz mode. For bridge motion, the payload mass affects the oscillation frequencies of the excited modes, as was shown in Figure 4.13. Therefore, a three-mode SI shaper was designed to suppress the swing, twist, and roll modes for payload masses ranging from 7 kg to 70 kg. Table 5.2 shows the parameters used for the SI shaper design. The bridge motion shaper is:

$$\begin{bmatrix} t(ms) \\ A \end{bmatrix} = \begin{bmatrix} 0 & 584 & 1157 & 1728 & 2298 \\ 0.196 & 0.216 & 0.237 & 0.198 & 0.153 \end{bmatrix} \tag{5.4}$$

The following data were collected for each test run:

- Test number
- Bridge move distance
- Trolley move distance
- Controller setting (e.g., shaped or unshaped)
- Course completion Time, t_c
- Number of obstacle collisions
- Number of button pushes

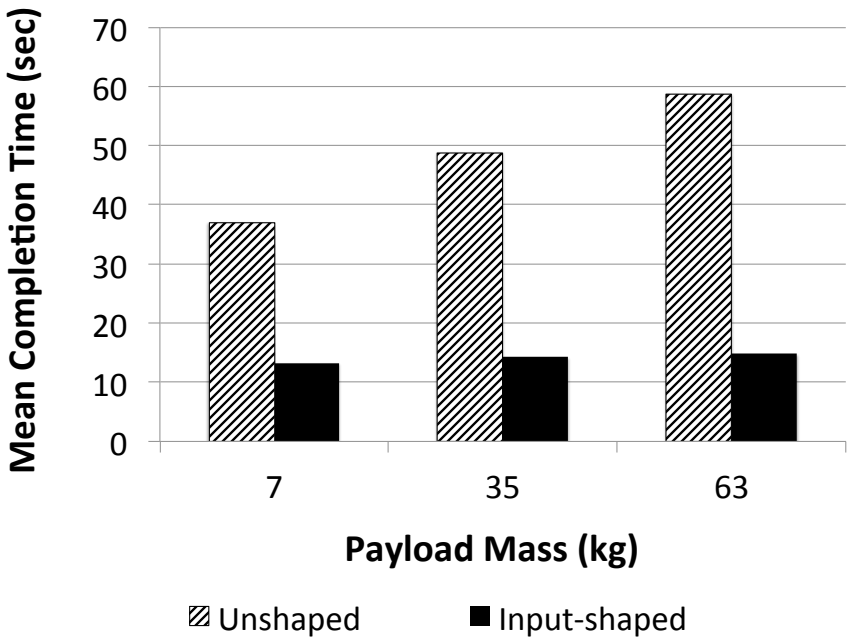

Figure 5.14: Average Completion Time Vs. Payload Mass

The data required to compute the number of button pushes were not recorded for test subjects 4 and 5.

5.4.1 Payload Mass, Bridge, and Trolley Study Results

Figure 5.14 shows the average course completion time for each of the three payload masses. For both the input-shaped and unshaped conditions, the average course completion time increases with the payload mass. The largest contributor to the total oscillation response is from the lowest-frequency "swing" mode. The "swing" mode damping ratio decreases as the payload mass is increased. Because most test runs must wait for the residual payload oscillation to decay so that the payload remains within the target area, this decrease in the "swing" mode damping ratio results in a longer average course completion time. Using a two-way ANOVA, there was a statistically significant interaction between the selected controller (unshaped vs. shaped) and the payload mass $[F(2, 114) = 8.33, p = 0.0004]$.

Figure 5.15 shows the average unshaped and input-shaped completion times for the 12 operators in the PMBT study. Input shaping decreased completion times by

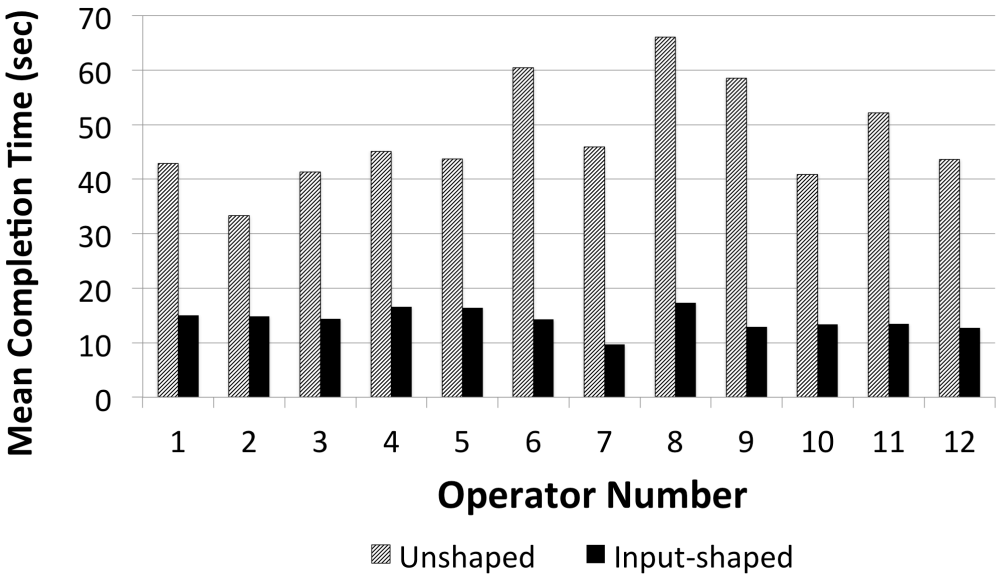

Figure 5.15: Average Completion Times for Operators in PMBT Study

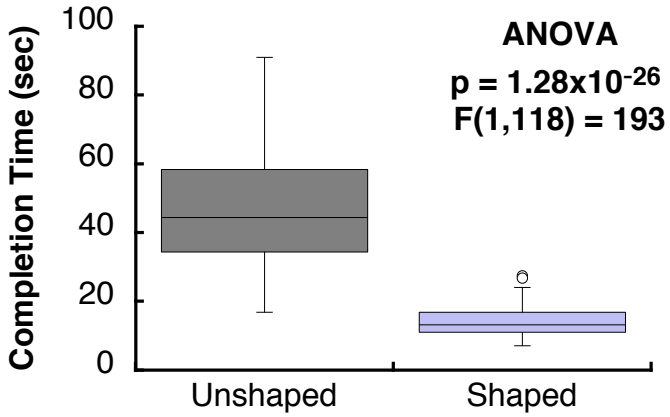

Figure 5.16: Box Plot of PMBT Study Completion Times

an average of 69%. A box plot of the completion times for all PMBT test runs is shown in Figure 5.16. The mean and standard deviation for the shaped and unshaped data is 14 ± 4 s and 47 ± 18 s, respectively.

A one-way ANOVA was performed to determine if differences between the input-shaped and unshaped means were statistically significant. Input shaping had a significant effect on completion time at the $p < 0.0001$ level for the two conditions tested $[F(1, 118) = 193, p = 1.28 \times 10^{-26}]$.

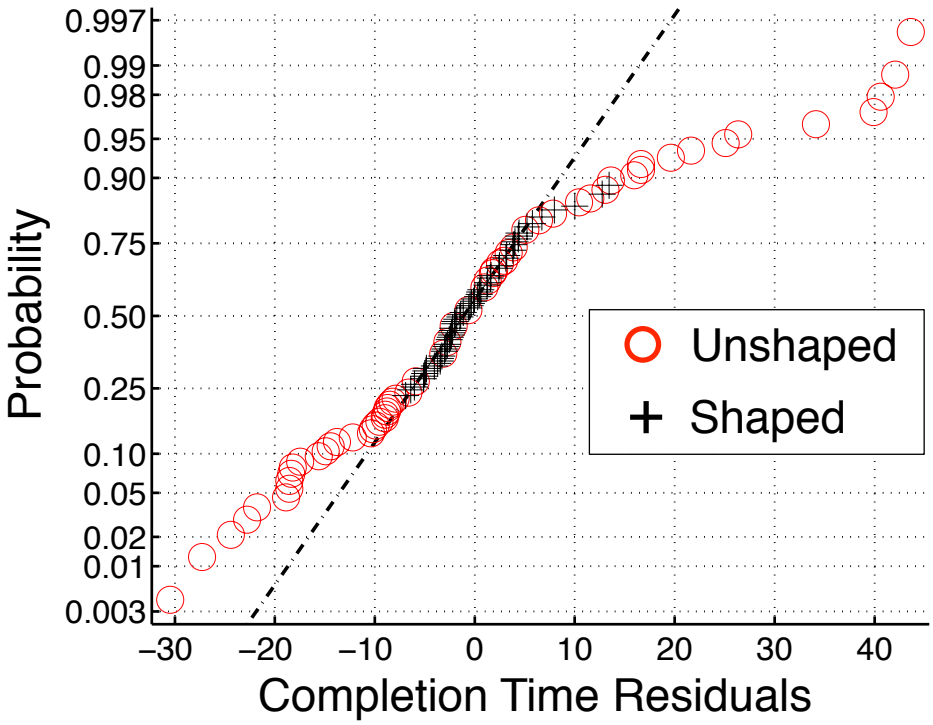

Figure 5.17: PMBT Study Completion Time Residuals

The completion time residuals were computed for both the unshaped and input-shaped data. The results are plotted in Figure 5.17. If the data points fall on a line, then the data represents a normal distribution. From the graph, it is apparent that the shaped data closely represents a normal distribution except for those points with the highest residuals. However, the unshaped data diverges from the fitted line for the points with the highest and lowest residuals. This indicates that the unshaped completion time residuals, when analyzed together with the shaped completion time residuals, are not best described as a normally distributed data set.

There are two reasons that may explain why the unshaped data diverges from the normal distribution. The first reason is the decreased separation distance between the two obstacles. This significantly increased the difficulty for navigating the payload between the two obstacles, especially with the large payload swing that can occur without the aid of input shaping. In some situations, the operators waited for large payload oscillations that were the result of trolley motions to decay before attempting

to move the payload between the obstacles. In other situations, the payload oscillations were small enough that the payload could be immediately moved between the two obstacles. In fact, there were 20 instances where the payload collided with one of the obstacles during the PMBT study when the standard crane controller was being used. However, the operators could immediately begin moving the payload between the obstacles when input shaping was used to suppress the payload oscillations. No collisions occurred when input shaping was enabled.

The second reason that could have contributed to the data diverging from a normal distribution is the different payload masses used in the PMBT study. The "swing" mode damping ratio decreases as the payload mass is increased, which results in larger residual oscillation amplitudes and smaller oscillation decay rates. If the payload had a large residual amplitude after the operator centered the payload within the target area, then the operator had to wait for the oscillations to decay and remain within the boundary before time was called. However, different payload masses were used in the PMBT study, so this waiting time was affected by the particular payload mass that was used. Also, a certain sequence of commands may have resulted in perfect cancellation of the modes after the payload was moved in the target area that resulted in an abnormally fast completion time.

The average number of button pushes to complete the obstacle course for each operator is shown in Figure 5.18. As mentioned before, the number of button pushes was not recorded for subjects 4 and 5. The average number of button pushes used for unshaped test runs was significantly higher for Subject 8 in comparison to the other participants. Most subjects moved the crane such that the oscillating payload was centered inside the target area and then waited for oscillations to naturally decay within the target area boundary. The increase in unshaped button pushes could be because Subject 8 was attempting to dampen out payload oscillations by using additional crane movements instead of waiting for the oscillations to naturally decay.

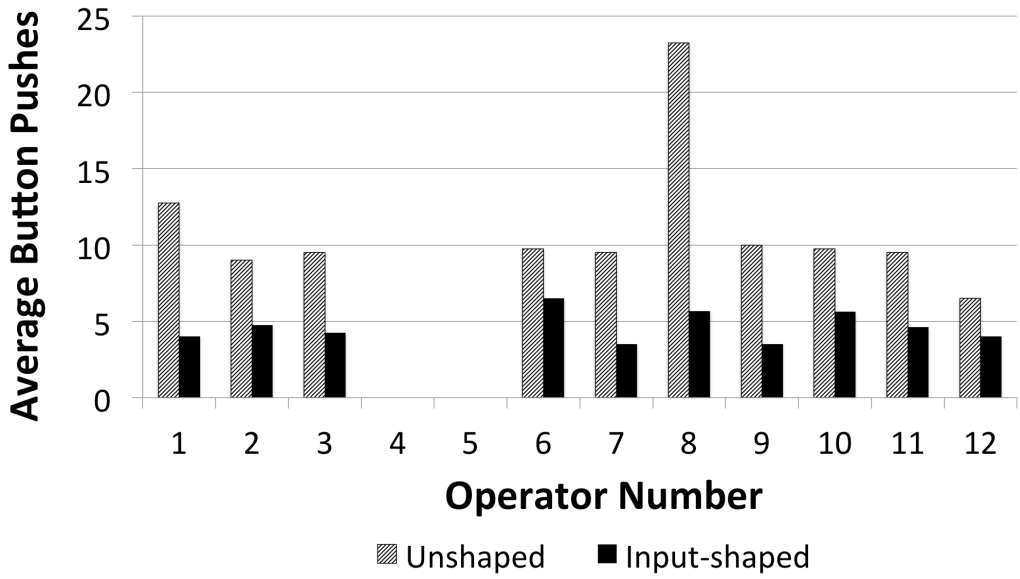

Figure 5.18: Average Number of Button Pushes

Excluding operators 4, 5, and 8, input shaping resulted in a 52% reduction in operator effort as indicated by the number of button pushes required to complete the obstacle course. Including the button-push data from operator 8, the percent reduction in operator effort increases slightly to 54%.

Multiple cranes are often used to maneuver large, distributed payloads. The payload geometry and rigging configuration may result in a multi-mode response that increases the complexity of the move. An input shaper can be designed to suppress the modes that cause unacceptable levels of oscillation. Studies of human operators driving a 2-ton industrial dual-hoist bridge crane carrying a triangular payload demonstrated that input shaping significantly improves task completion time. Furthermore, input-shaping control greatly decreased operator effort, as measured by the number of interface button pushes needed to complete a task. These results clearly demonstrate the benefit of input-shaping control on dual-hoist bridge cranes.

CHAPTER VI

CONCLUSIONS

Crane motion induces payload oscillation that makes accurate positioning of the payload a challenging task. Excessive payload sway can result in collisions that damage equipment or injure people. A large payload that swings outward from the base of a crane can also greatly increase the tipping moment and lead to catastrophic collapse of the crane. As the payload size increases, it may be necessary to utilize multiple cranes for better control of the payload orientation and position. However, simultaneously maneuvering multiple cranes to transport a single payload increases the complexity and danger of the operation.

This thesis investigated the dynamics and control of dual-hoist bridge cranes transporting distributed payloads and introduced a new Input-Shaped System Identification method to aid in the dynamics investigation. A new kind of input shaper, called a Selective Mode Amplification (SMA) shaper, was developed in Chapter 2 to suppress all but one mode to a low level. In this regard, the SMA shaper is a type of band-pass filter where the passed frequencies are amplified as much as possible, rather than passed with a unity gain. The SMA shaper can also be used to bring a small-amplitude mode to light by modifying one of the vibration constraints. This feature was demonstrated in simulation by using SMA shapers to amplify one of the three modes induced from moving a dual-hoist bridge crane in the bridge direction.

In Chapter 3, a new system identification method, called Input-Shaped System Identification, was developed that utilizes input shaping for determining the frequencies and amplitudes of the individual modes of a multi-mode system. The system identification method consists of a frequency identification process and an amplitude

identification process.

The frequency identification process uses a FFT of the measured response to determine the modal frequencies after the system has been moved with it's own actuators. Then, input shapers are designed to suppress the discovered modes in order to increase the signal-to-noise ratio of the measured response for the identification of additional modes.

The amplitude identification process uses SMA shapers designed to suppress all but one mode so that the measured response is primarily composed of the single mode of interest. Then, the amplitude of the remaining mode can be easily determined from the time response. This technique can be used to characterize the modal frequencies and amplitudes for various system configurations, which can be used to design input shapers that will be robust to expected system configurations and parameter variations.

In Chapter 4, a dynamic model of a dual-hoist bridge crane was used to investigate the hook and payload oscillations originating from trolley and bridge motions. The modes excited from bridge and trolley motions were identified, and simulations were completed to determine how the frequency and amplitude of the three modes induced by bridge motion change in response to variations in the payload mass and geometry. Insights from this dynamic analysis were used to design input shapers that reduce payload oscillation originating from bridge and trolley motions.

Most cranes are driven by human operators. For this reason, it is important to understand how input shaping affects human performance when completing practical crane tasks if input shaping is to be used in multi-crane scenarios where humans are generating the commands. In Chapter 5, human operators drove an industrial 2-ton dual-hoist bridge crane carrying a triangular payload through an obstacle course in order to investigate the effect input shaping has on task performance. Three studies were completed requiring operators to transport the payload between two

locations for various trolley and bridge move distances and payload masses. In each study, input-shaping significantly improved the task completion time. Furthermore, input-shaping control greatly decreased operator effort, as measured by the number of button pushes needed to complete a task. These results clearly demonstrate the benefit of input-shaping control on dual-hoist bridge cranes.

6.1 Future Work

This thesis used Input-Shaped System Identification to characterize the modes of a dual-hoist bridge crane for variations in the mass and width of a triangular payload and for variations in the width ratio of a right-trapezoidal payload. However, there are other system parameters that could be investigated, such as the suspension cable lengths and trolley separation distance, using these two payloads. Other kinds of distributed payloads could be investigated. For example, only flat plates were considered. The effect of the payload thickness could also be researched.

The dual-hoist bridge crane can also be used to transport an active payload, such as a painting robot. A painting robot located in the Boeing Lab has an arm that can be controlled to move a painting mechanism attached to an end effector. In this scenario, both the robotic arm and the crane can be moved to reposition the end effector. If the robotic arm is used to move the end effector, then the payload's center of mass changes and causes a small disturbance. Investigations could be completed to analyze the dynamic effects that can originate from this type of active payload.

This thesis used input shaping to reduce motion-induced payload oscillations. However, external disturbances can also cause payload oscillations. For example, payload oscillations can occur if the crane and payload configuration is not initially in static equilibrium immediately after lifting the payload from the ground. A feedback controller could be developed for dual-hoist bridge cranes to aid operators in dealing with disturbances.

Physical systems are subject to damping forces. It was evident that the simulation results, which neglected damping, were significantly different than the experimental data for light triangular payloads that were moved in the bridge direction. Damping parameters were added to the dual-hoist bridge crane model, and simulations using this simple damping model provided results that were much closer to the experimental results. However, more sophisticated damping models could be investigated to improve the simulation accuracy.

APPENDIX A

DUAL-HOIST BRIDGE CRANE MODEL

The software package *MotionGenesis* [1] was used to create a numerical model for performing simulations of the dual-hoist bridge crane. The code was initially created by Maleki [12] for his dissertation. First, an equilibrium model was used to solve for the initial conditions of the system for the selected crane and payload configuration. Then, a dynamic model was used to generate the equations of motion for the dual-hoist bridge crane. The output for each of these *MotionGenesis* files was a code for performing dynamic simulations in MATLAB.

A.1 Equilibrium Model

```
SetAutoZee(ON)

%% Frames and Bodies
NewtonianFrame N % Newtonian reference frame
RigidFrame Cable1, Cable2 % Rigid, inflexible cables
RigidBody Link % Rigid payload between cables

% Two ends of rigid link, for convenience - also allows adding hook mass to sim
Point T1(Cable1), T2(Cable2)  % Trolleys
Particle P1, P2  % two ends of rigid link

% Variables and constants
Variable theta_1'', theta_2'',beta''% cables angles for trolley motion
Variable phi_1'',phi_2'',gamma''% cable angles for bridge motion
Variable psi''% payload rotation angle
Variable y1'', y2''% Trolley pos, vel, accel
Variable x1'', x2''% Bridge pos, vel, accel (same for both trolleys)
Constant LE+, LW+, LC+, g+ % cable lengths and gravity (limit to positive)
Constant MC+, ME+, MW+ % Masses (limit to positive)
Specified a_trol1, a_trol2, a_bridge % accel of trolleys & bridge is input
Constant B_cable1, B_cable2 % cable damping
Constant Ixx, Iyy, Izz, Ixy, Iyz, Izx % moments and products of inertia of payload
Constant LCx, LCy, LCz % distances to COM of payload

% Set derivatives of trolley motion
setDt( y1'' = a_trol1)
```

```
setDt( y2'' = a_trol2)
setDt( x1'' = a_bridge)
setDt( x2'' = a_bridge)

% Variables that are going to be in equations of motion
SetGeneralizedSpeed(theta_1',theta_2',beta',phi_1',phi_2',gamma', psi')

%----- Set intertial properties
% Payload mass and inertia
Link.SetMass(MC)
Link.SetInertia( LinkCM, Ixx, Iyy, Izz, Ixy, Iyz, Izx )

% Hook masses
P1.SetMass(ME)
P2.SetMass(MW)

%----- Kinematics and motion description
% Movement of the two trolleys
T1.Translate(No, x1*Nx> + y1*Ny>) % trolley 1
T2.Translate(No, x2*Nx> + y2*Ny>) % trolley 2

% Rotation of two cables
Cable1.Rotate(N, BodyXYZ, theta_1, phi_1, 0) % Cable 1 (E)
Cable2.Rotate(N, BodyXYZ, theta_2, phi_2, 0) % Cable 2 (W)

% Movement of hook/cable-link connections
P1.Translate(No,p_No_T1> - LE*Cable1z>)      % hook 1
P2.Translate(No,p_No_T2> - LW*Cable2z>)      % hook 2

Link.Rotate( N, BodyXYZ, beta, psi, gamma ) % payload
LinkCM.Translate( No, (p_No_P1> + LCx*Linkx> + LCy*Linky> + LCz*Linkz>) )

% Save hooks/cable-link connection for plotting/checking of Eq of Motion
P1_x = Dot( p_No_P1>, Nx> )
P1_y = Dot( p_No_P1>, Ny> )
P1_z = Dot( p_No_P1>, Nz> )

P2_x = Dot( p_No_P2>, Nx> )
P2_y = Dot( p_No_P2>, Ny> )
P2_z = Dot( p_No_P2>, Nz> )

% External Forces
System.AddForceGravity( -g*Nz> ) % gravity force

% Rotary damping between the trolleys and cable links
Cable1.AddTorque( -B_cable1 * Cable1.GetAngularVelocity(N) )
Cable2.AddTorque( -B_cable2 * Cable2.GetAngularVelocity(N) )

%------ Equations of motion
% Set up 4-bar linkage constraints in X, Y, Z directions.
% The velocity in each direction = 0
Dependent[1] = Dot( Dt(p_No_T1> - LE*Cable1z> + LC*Linky>
+ LW*Cable2z> - p_No_T2>, N), Nx>)
Dependent[2] = Dot( Dt(p_No_T1> - LE*Cable1z> + LC*Linky>
```

```
+ LW*Cable2z> - p_No_T2>, N), Ny>)
Dependent[3] = Dot( Dt(p_No_T1> - LE*Cable1z> + LC*Linky>
+ LW*Cable2z> - p_No_T2>, N), Nz>)

% Implement constraint equations (basically 4-bar with moving connections)
Constrain(Dependent[theta_2', beta', gamma'])

% Kane's method dynamics - gives equations of motion
Dynamics = System.GetDynamicsKane()
Solve( Dynamics, theta_1'', phi_1'', phi_2'', psi'')

% Get equilibrium conditions
eq[1] = Dot(p_No_T1> - LE*Cable1z> + LC*Linky>
+ LW*Cable2z> - p_No_T2>, Nx>)
eq[2] = Dot(p_No_T1> - LE*Cable1z> + LC*Linky>
+ LW*Cable2z> - p_No_T2>, Ny>)
eq[3] = Dot(p_No_T1> - LE*Cable1z> + LC*Linky>
+ LW*Cable2z> - p_No_T2>, Nz>)
% Expression for the torque generated about P1 in the YZ plane (about the x axis)
eq[4] = 0.5*g*LE*(2*ME*sin(theta_1)+2*MW*sin(theta_2)*cos(beta-theta_1)/cos(beta-
theta_2)+MC*(2*sin(theta_1)-cos(beta)*sin(theta_1-theta_2)/cos(beta-theta_2)))

% Constant values - constraints for the linkages.
Input LE = 2 m, LW = 2 m, LC = 3 m, MC = 10 kg, ME = 10 kg, MW = 10 kg
Input x1 = 0 m, x2 = 0 m, x1' = 0 m/s, x2' = 0 m/s
Input y1 = 0 m, y2 = 3 m, y1' = 0 m/s, y2' = 0 m/s
Input g = 9.81 m/s^2
Input B_cable1 = 0.0, B_cable2 = 0.0

% Initial conditions
Input theta_1 = 15 deg, theta_2 = 15 deg, beta = 0 deg, phi_1 = 0 deg
Input phi_2 = 0 deg, gamma = 0 deg, psi = 0 deg % These are used as initial guesses.

% Generate MATLAB code
CODE Nonlinear(eq, theta_1, theta_2, beta, gamma) two_crane_planar_equil_3d.m
```

A.2 Dynamic Model

```
SetAutoZee(ON)

%% Frames and Bodies
NewtonianFrame N % Newtonian reference frame
RigidFrame Cable1, Cable2 % Rigid, inflexible cables
RigidBody Link % Rigid payload between cables

% Two ends of rigid link, for convenience - also allows adding hook mass to sim
Point T1(Cable1), T2(Cable2)  % Trolleys
Particle P1, P2  % two ends of rigid link
```

```
% Variables and constants
Variable theta_1'', theta_2'',beta''% cables angles for trolley motion
Variable phi_1'',phi_2'',gamma''% cable angles for bridge motion
Variable psi''% payload rotation angle
Variable y1'', y2''% Trolley pos, vel, accel
Variable x1'', x2''% Bridge pos, vel, accel (same for both trolleys)
Constant LE+, LW+, LC+, g+ % cable lengths and gravity (limit to positive)
Constant MC+, ME+, MW+ % Masses (limit to positive)
Specified a_trol1, a_trol2, a_bridge % accel of trolleys & bridge is input
Constant B_cable1, B_cable2 % cable damping
Constant B_payload % payload damping due to wind
Constant Ixx, Iyy, Izz, Ixy, Iyz, Izx % moments and products of inertia of payload
Constant LCx, LCy, LCz % distances to COM of payload

% Set derivatives of trolley motion
setDt( y1'' = a_trol1)
setDt( y2'' = a_trol2)
setDt( x1'' = a_bridge)
setDt( x2'' = a_bridge)

% Variables that are going to be in equations of motion
SetGeneralizedSpeed(theta_1',theta_2',beta',phi_1',phi_2',gamma', psi')

%----- Set intertial properties
% Payload mass and inertia
Link.SetMass(MC)
Link.SetInertia( LinkCM, Ixx, Iyy, Izz, Ixy, Iyz, Izx )

% Hook masses
P1.SetMass(ME)
P2.SetMass(MW)

%----- Kinematics and motion description
% Movement of the two trolleys
T1.Translate(No, x1*Nx> + y1*Ny>) % trolley 1
T2.Translate(No, x2*Nx> + y2*Ny>) % trolley 2

% Rotation of two cables
Cable1.Rotate(N, BodyXYZ, theta_1, phi_1, 0) % Cable 1 (E)
Cable2.Rotate(N, BodyXYZ, theta_2, phi_2, 0) % Cable 2 (W)

% Movement of hook/cable-link connections
P1.Translate(No,p_No_T1> - LE*Cable1z>)      % hook 1
P2.Translate(No,p_No_T2> - LW*Cable2z>)      % hook 2

Link.Rotate( N, BodyXYZ, beta, psi, gamma ) % payload
LinkCM.Translate( No, (p_No_P1> + LCx*Linkx> + LCy*Linky> + LCz*Linkz>) )

% Save hooks/cable-link connection for plotting/checking of Eq of Motion
P1_x = Dot( p_No_P1>, Nx> )
P1_y = Dot( p_No_P1>, Ny> )
P1_z = Dot( p_No_P1>, Nz> )

P2_x = Dot( p_No_P2>, Nx> )
```

```
P2_y = Dot( p_No_P2>, Ny> )
P2_z = Dot( p_No_P2>, Nz> )

% External Forces
System.AddForceGravity( -g*Nz> ) % gravity force

% Rotary damping between the trolleys and cable links
Cable1.AddTorque( -B_cable1 * Cable1.GetAngularVelocity(N) )
Cable2.AddTorque( -B_cable2 * Cable2.GetAngularVelocity(N) )

% Viscous damping due to wind resistance against payload
LinkCM.addForce( -B_payload * Dot( LinkCM.getVelocity(N), Linkx>) * Linkx>)

%------ Equations of motion
% Set up 4-bar linkage constraints in X, Y, Z directions.
% The velocity in each direction = 0
Dependent[1] = Dot( Dt(p_No_T1> - LE*Cable1z> + LC*Linky>
+ LW*Cable2z> - p_No_T2>, N), Nx>)
Dependent[2] = Dot( Dt(p_No_T1> - LE*Cable1z> + LC*Linky>
+ LW*Cable2z> - p_No_T2>, N), Ny>)
Dependent[3] = Dot( Dt(p_No_T1> - LE*Cable1z> + LC*Linky>
+ LW*Cable2z> - p_No_T2>, N), Nz>)

% Implement constraint equations (basically 4-bar with moving connections)
Constrain(Dependent[theta_2', beta', gamma'])

% Kane's method dynamics - gives equations of motion
Dynamics = System.GetDynamicsKane()
Solve( Dynamics, theta_1'', phi_1'', phi_2'', psi'')

%----- Setup parameters to pass to Matlab Code
% Integration parameters
Input  tFinal=10,      integStp=0.02,    absError=1.0E-07,  relError=1.0E-07

% Constant values
Input LE = 2 m, LW = 2 m, LC = 3 m, MC = 10 kg, ME = 10 kg, MW = 10 kg
Input x1 = 0 m, x2 = 0 m, x1' = 0 m/s, x2' = 0 m/s
Input y1 = 0 m, y2 = 3 m, y1' = 0 m/s, y2' = 0 m/s
Input g = 9.81 m/s^2
Input B_cable1 = 0.0, B_cable2 = 0.0

% Initial conditions
Input theta_1 = 0 deg, theta_2 = 0 deg, theta_1' = 0 deg/sec
Input theta_2' = 0 deg/sec, beta = 0 deg
Input phi_1 = 0 deg, phi_2 = 0 deg, phi_1' = 0 deg/sec
Input phi_2' = 0 deg/sec, gamma = 0 deg
Input psi = 0 deg, psi' = 0 deg/sec

% Quantities to output
Output t, x1 m, x2 m, y1 m, y2 m, P1_x m, P1_y m, P2_x m, P2_y m, theta_1 deg
Output theta_2 deg, beta deg, theta_1' deg/sec, theta_2' deg/sec, beta' deg/sec
Output phi_1 deg, phi_2 deg, gamma deg, phi_1' deg/sec, phi_2' deg/sec
Output gamma' deg/sec, psi deg, psi' deg/sec
```

```
% Create MATLAB code
ODE() two_crane_planar_3d_PayloadDamping.m

% Save MotionGenesis Output
save two_crane_planar_3d.all
```

REFERENCES

[1] *MotionGenesis*. http://www.motiongenesis.com/.

[2] Abdel-Rahman, E. M., Nayfeh, A. H., and Masoud, Z. N., "Dynamics and control of cranes: A review," *JVC/Journal of Vibration and Control*, vol. 9, no. 7, pp. 863 – 908, 2003.

[3] Bailes, D., "Lifting loads with more than one lifting machine," tech. rep., Hoist Magazine, September 2009.

[4] Ewins, D., *Modal Testing: Theory, Practice and Application, 2nd Edition*. Research Studies Press Ltd., 2 ed., 2000.

[5] Gloth, G. and Sinapius, M., "Analysis of swept-sine runs during modal identification," *Mechanical Systems and Signal Processing*, vol. 18, 2004.

[6] He, J. and Fu, Z.-F., *Modal Analysis*. No. 9780750650793, Oxford ; Boston : Butterworth-Heinemann, 2001.

[7] Huang, J., Xie, X., and Liang, Z., "Control of bridge cranes with distributed-mass payload dynamics.," *IEEE/ASME Transactions on Mechatronics*, vol. 20, no. 1, p. 481, 2015.

[8] Hyde, J. M. and Seering, W. P., "Inhibiting multiple mode vibration in controlled flexible systems," in *American Control Conf.*, (Boston, MA), 1991.

[9] Karaagacli, T., Yildiz, E. N., and Nevzat Ozguven, H., "A new method to determine dynamically equivalent finite element models of aircraft structures from modal test data.," *Mechanical Systems and Signal Processing*, vol. 31, pp. 94 – 108, 2012.

[10] Kim, D. and Singhose, W., "Performance studies of human operators driving double-pendulum bridge cranes," *Control Engineering Practice*, vol. 18, no. 6, pp. 567–576, 2010.

[11] Krabbendam, R., "Tandem lift goes wrong." URL: www.heavyliftnews.com/news/tandem-lift-goes-wrong, June 2014.

[12] Maleki, E., *Control of Human-Operated Machinery with Flexible Dynamics*. PhD thesis, Georgia Institute of Technology, 2013.

[13] Rudroju, S., Gupta, A., and Yandamuri, S., "Operational modal analysis of aluminum beams," *Journal of the IEST*, vol. 50, no. 1, pp. 74 – 85, 2007.

[14] Schwarz, B. J. and Richardson, M. H., "Experimental modal analysis," in *Vibrant Technology*, CSI Reliability Week, Orlando, FL, 1999.

[15] Singer, N. C. and Seering, W. P., "An extension of command shaping methods for controlling residual vibration using frequency sampling," in *IEEE International Conference on Robotics and Automation*, (Nice, France), 1992.

[16] Singer, N. C. and Seering, W. P., "Preshaping command inputs to reduce system vibration," *ASME J. of Dynamic Sys., Measurement, and Control*, vol. 112, no. March, pp. 76–82, 1990.

[17] Singh, J. P., Agarwal, P., Kumar, A., and Thakkar, S. K., "Identification of modal parameters of a multistoried RC building using ambient vibration and strong vibration records of Bhuj earthquake, 2001.," *Journal of Earthquake Engineering*, vol. 18, no. 3, pp. 444 – 457, 2014.

[18] Singhose, W. E., Crain, E. A., and Seering, W. P., "Convolved and simultaneous two-mode input shapers," *IEE Control Theory and Applications*, vol. 144, pp. 515–220, 1997.

[19] Singhose, W. and Seering, W., *Command Generation for Dynamic Systems*. No. 978-0-9842210-0-4, Lulu, August 2011.

[20] Singhose, W., Seering, W., and Singer, N., "Residual vibration reduction using vector diagrams to generate shaped inputs," *ASME J. of Mechanical Design*, vol. 116, no. June, pp. 654–659, 1994.

[21] Singhose, W., Seering, W., and Singer, N., "Input shaping for vibration reduction with specified insensitivity to modeling errors," in *Japan-USA Sym. on Flexible Automation*, (Boston, MA), 1996.

[22] Smith, O. J. M., "Posicast control of damped oscillatory systems," *Proceedings of the IRE*, vol. 45, no. 9, pp. 1249–1255, 1957.

[23] Soria, L., Peeters, B., Anthonis, J., and der Auweraer, H. V., "Operational modal analysis and the performance assessment of vehicle suspension systems," *Shock and Vibration*, vol. 19 Issue 5, pp. 1099–1113, 2012.

[24] Vayssettes, J., Mercere, G., Vacher, P., and Callafon, R. D., "Frequency-domain identification of aircraft structural modes from short-duration flight tests.," *International Journal of Control*, vol. 87, no. 7, pp. 1352 – 1372, 2014.

[25] www.osha.gov, "Employee is injured when crane tips over," Tech. Rep. Inspection: 314671298, Occupational Safety and Health Administration, June 2010.

[26] www.vertikal.net, "Tandem lift overturn in Caracas." URL: www.vertikal.net/en/news/story/19048/, December 2013.

[27] WWW.VERTIKAL.NET, "Crane dropped in tandem lift." URL: http://www.vertikal.net/en/news/story/22085/, February 2015.

[28] ZAMEROSKI, D., STARR, G., WOOD, J., and LUMIA, R., "Rapid swing-free transport of nonlinear payloads using dynamic programming," *ASME Journal of Dynamic Systems, Measurement, and Control*, vol. 130, no. 4, p. 041001, 2008.

[29] ZWOLSKI, J. and BIEŃ, J., "Modal analysis of bridge structures by means of forced vibration tests," *JOURNAL OF CIVIL ENGINEERING AND MANAGEMENT*, vol. 17(4), pp. 590–599, 2011.